Quantifying nearshore bathymetric change using an Unoccupied Surface Vehicle equipped with RTK-GNSS and echosounder: A case study in the Neuse River Estuary, NC

By

Ryann Knowles

July 2022

Director of Thesis: Dr. Hannah Sirianni

Major Department: Geography, Planning, and Environment

The Neuse River Estuary (NRE) located in eastern North Carolina is experiencing shoreline bluff retreat and corresponding nearshore bathymetric change due to an increase in intense storm events such as hurricanes. Monitoring changes in nearshore bathymetry can aid in understanding sediment flux for management and restoration purposes. New remote sensing devices such as small Unoccupied Surface Vehicles (sUSV) allow for on-demand repeat bathymetric surveys of shallow nearshore environments where larger vessels cannot reach. This study uses a sUSV equipped with a single beam echosounder to investigate nearshore morphological changes in the Neuse River Estuary. Two Real-time Kinematic Global Navigation Satellite Systems (RTK-GNSS) and sUSV surveys were carried out in February and April 2022. For each of the two surveys, three Bathymetric Elevation Models (BEMs) were generated using Empirical Bayesian Kriging (EBK), Global Polynomial Interpolation (GPI), and Spline. EBK achieved the best result for both surveys based on conditions observed in the field as well as a vertical Root Mean Square Error (RMSE) of 0.21 m for February and 0.16 m for April. Wave and weather sensors were installed for this study to help determine potential causes of morphological changes. While both months had similar average wind speeds (average 5-10 m/s), their directions were different (Northeast and South directions for February and Southwest direction for April). As can be

expected in a wave dominated estuary with these observed wind speeds, 90th percentile wave depth minimum and maximum ranged 0.05 m February and 0.03 m for April. Short term changes in the nearshore bathymetry were negative resulting in erosion with no estimated deposition. Bathymetry loss ranged from 0.3 to 0.69 m between February and April, and the observed wind and wave data indicate these changes were likely due to another contributing factor such as currents. To assist future work using sUSVs in shallow nearshore estuarine environments, a workflow of best practices when conducting sUSV surveys was developed in this study. It is anticipated that the results from this study will useful information for researchers conducting sUSV surveys as well as the causes of nearshore morphological change in shallow estuarine environments.

Quantifying nearshore bathymetric change using an Unoccupied Surface Vehicle equipped with RTK-GNSS and echosounder: A case study in the Neuse River Estuary, NC

A Thesis

Presented To the Faculty of the Department of Geography, Planning, and Environment

East Carolina University

In Partial Fulfillment of the Requirements for the Degree

Master of Science in Geography

by

Ryann Knowles

July, 2022

Quantifying nearshore bathymetric change using an Unoccupied Surface Vehicle equipped with RTK-GNSS and echosounder: A case study in the Neuse River Estuary, NC

By

Ryann Knowles

APPROVED BY:

Director of Thesis _____
Hannah Sirianni, PhD

Committee Member _____
Scott Lecce, PhD

Committee Member _____
Thad Wasklewicz, PhD

Chair of the Department of Geography, Planning and the Environment _____
(Jeff Popke, Ph.D.)

Interim Dean of the Graduate School _____
Kathleen Cox, PhD

DEDICATIONS

This work is dedicated to my dog, Archie Lou. He spent many nice weather days looking out the window watching other dogs play ball. Despite this, he was always wagging his tail providing the best support a woman's best friend could ever offer.

ACKNOWLEDGMENTS

I would like to thank my advisor, Dr. Hannah Sirianni, and committee members, Dr. Scott Lecce, and Dr. Thad Wasklewicz. I appreciate the lab members and other individuals who spent their free time assisting me in the field.

TABLE OF CONTENTS

LIST OF TABLES

LIST OF FIGURES

LIST OF EQUATIONS

Chapter 1: Introduction

1.1 Significance of Monitoring Nearshore Changes in Estuarine Systems

Estuarine environments are complex semi-enclosed coastal systems that receive direct inputs from both the head of a river and the mouth of a sea. Estuaries are highly dynamic due to a unique combination of geological history, waves and tides, weather conditions, currents (Laird et al., 1975), and human modifications to the shoreline. These natural and human coastal processes combined with a changing climate influence sediment fluxes and morphological changes within the shore topography (land at the edge of the estuary water) and nearshore bathymetry (seabed close to the shore). As sea levels are rising and strong storm events are occurring more often, estuarine systems are becoming critical areas of interest for sediment loss (e.g., Corbett, 2010), coastal planning and management (Horta et al., 2014), and navigation purposes (El-Hattab, 2014). Understanding how the forcing agents of waves shape nearshore morphology, and how nearshore morphologies shape waves is important when monitoring dynamic estuarine environments. Monitoring morphological changes in the nearshore estuarine environment first requires data of the seabed topography captured at two or more-time intervals (relative to an established vertical coordinate system). Bathymetric models are then generated from each dataset and overlain with one another in a Geographic Information System (GIS) to calculate or differentiate any morphological changes between them. Recently, affordable, and effective on-demand nearshore bathymetry mapping and monitoring devices such as small Unoccupied Surface Vehicles (sUSV) are available to researchers to survey hard-to-reach areas (e.g., Specht et al., 2020). sUSVs have the potential to assist researchers with real-time monitoring of nearshore morphological change due to forcing agents such as winds and waves

1.2 Characteristics of Estuarine Environments

1.2.1 Dynamics of Estuaries

Estuarine systems have similar energy dynamics, where freshwater from rivers mix with saltwater from the sea. Their complexity can be simplified as three zones based on three energy levels, as shown in Figure 1 (Dalrymple et al., 1992). These include: 1) the outer zone which is marine-dominated by waves and tides (light blue), 2) the central zone which is a mix of river-dominated and marine-dominated processes (light red), and 3) the inner zone where the river source empties into the estuary and is considered river-dominated (light green) (Figure 1). The marine-dominated outer zone at the mouth and river-dominated inner zone at the head are high-energy areas where course sediments move easier. This leaves a low-energy central zone where fine sediments settle and thus muds typically accumulate (Dalrymple et al., 1992). While the complexity of estuaries can be simplified into three zones based on energy levels from river and marine processes, the characteristic of each estuary is unique.

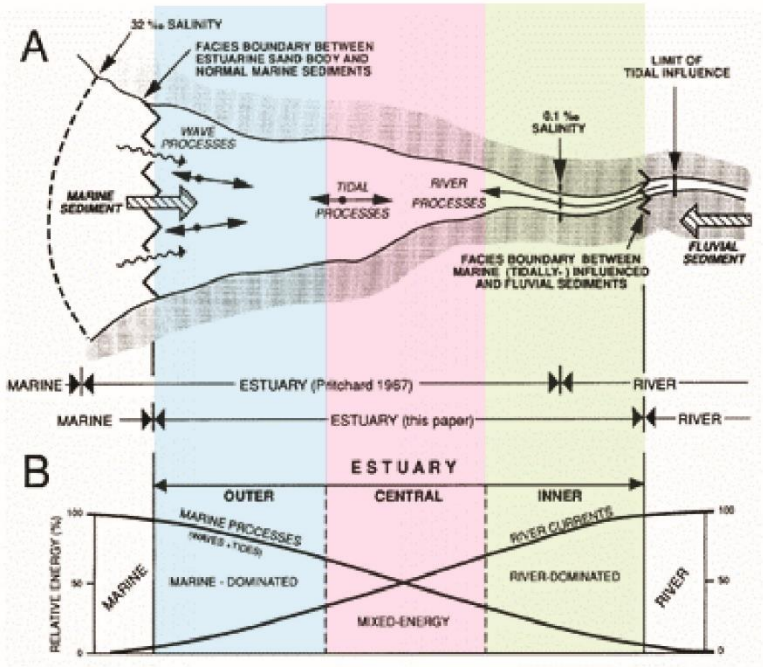

Figure 1. (A) birds eye view of the estuarine system. (B) chart of the differing energies in the three zones defined by outer (light blue), central (light red), and inner (light green). The estuary is the central zone. Figure modified from Dalrymple et al. (1992).

1.2.2 Geological History of Estuaries

The characteristics of estuaries are ordered by their interesting landforms, which largely depend on the geological history, influence of waves or tides, weather conditions, and currents (Laird et al., 1975). The shape and extent of estuaries are determined by geological history. The geology of an estuary is classified into four major types including bar-built, tectonic, fjords, and drowned river valley, as described by (NOAA, 2021). The four types of estuaries can be further split into two groups. The first is where differing energies from the river and sea flow without blockage by aquatic sills or landforms at the river mouth. On the other hand, the second group is where river and sea processes are disrupted by aquatic sill or landforms.

Tectonic and drowned river valley estuaries fall into the first group as fresh and saltwater mix within these estuaries without obstruction by topographic and bathymetric barriers. Tectonic

estuaries were formed by tectonic activity. A tectonic estuary typically occurs near fault lines when earthquakes take place and leave the earth's crust to subside, which produces a basin that fills with freshwater from the river and saltwater from the sea (NOAA, 2021). An example of a tectonic estuary is the San Francisco Bay, California (Elder, 2013). Drowned river valley estuaries on the other hand were existing river valleys that flooded during the end of the last ice age (10,000-18,000 years ago) when melting glaciers caused sea levels to rise (NOAA, 2021). They are found on low-lying coastal plains such as the East Coast of the US including Chesapeake Bay in Maryland and Virginia, and the Neuse River Estuary in North Carolina.

Fjord and bar-built estuaries fall into the second group because the mouth of the estuary is typically semi-blocked by aquatic sills or barrier islands. Fjord estuaries are narrow steep river valleys carved by advancing glaciers that were later flooded by seawater as the glaciers retreated. The advance and retreat of glaciers formed aquatic sills (i.e., relatively shallow seafloor barriers) at the river mouth of fjord estuaries, which allows for larger amounts of freshwater input from the river versus lower amounts of saltwater input from the sea (Harris, 2012; NOAA, 2021). Fjords are found where glaciers advanced, such as Glacier Bay in Alaska and the Puget Sound, Washington, USA. Bar-built estuarine systems on the other hand occur when sand bars or barrier islands are created by ocean wave and current interactions along the coast, which is fed by rivers or streams that have little water flow to the estuary (NOAA, 2021). This minimal input from rivers with the mouth blocked by barrier islands causes a lagoon to form, which is a calm water feature between the coast and the barrier beach or island features. Wash-over events can occur on the bar features during a severe storm event and can open the mouth of the estuary leaving the once protected lagoon and coast open to hazards, animal migration, and changing water levels

(NOAA, 2021; Orescanin et al., 2021). The Albemarle Pamlico Sound in North Carolina is an example of bar-built estuarine system.

1.2.3 Wave and Tide-dominated Estuaries

Estuarine systems are also defined by the influence of tides or waves. Tide-dominated estuaries rely on tides to construct the sediment movement through the estuary (R. Davidson-Arnott, 2011). Tides occur due to the rise and fall of sea level from the gravitational pull between the Earth, sun, and moon. In tide-dominated estuaries (see Figure 2), the outer zone (light blue) is influenced by tide interactions where tidal influence increases in the direction of the inner zone and the tidal energy dominates the wave energy (Dalrymple et al., 1992; Laird et al., 1975). The outer zone of tide-dominated coasts also may contain sand bars and mudflats (light blue in Figure 2). Conversely, wave-dominated estuarine systems are where tidal actions are not dominant. Wave-dominated coasts evolve through erosion, transport, and deposition of sediment associated with waves and wave-dominated currents (Davidson-Arnott, 2011). Unlike tide-dominated estuaries, the outer zone is dominated strongly by wave interactions, and the interactions decrease in the direction of the inner zone (Dalrymple et al., 1992). Wave-dominated estuaries are also different in that they include a barrier island formation in the outer zone (light blue in Figure 3). Barrier islands block the estuary from direct contact with wave energy from the open ocean until they are disrupted by intense storm and wash over events that cause greater wave interaction within the estuary (Dalrymple et al., 1992). While tide-dominated estuaries rely on tides being the dominant influence that drives changes within the system, wave-dominated estuaries rely on waves.

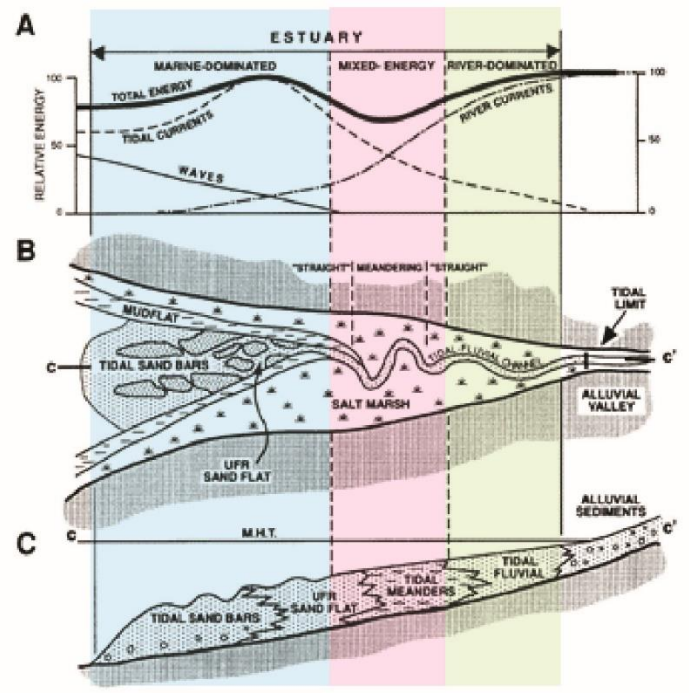

Figure 2. (A) differing energies within the tide-dominated estuarine system. (B) birds-eye view of the estuarine system. (C) cross-sectional view of the estuarine system stratigraphy. The marine-dominated zone is shown in light blue, the mixed energy zone is shown in light red, and the river-dominated zone is shown in light green. Figure modified from Dalrymple et al. (1992).

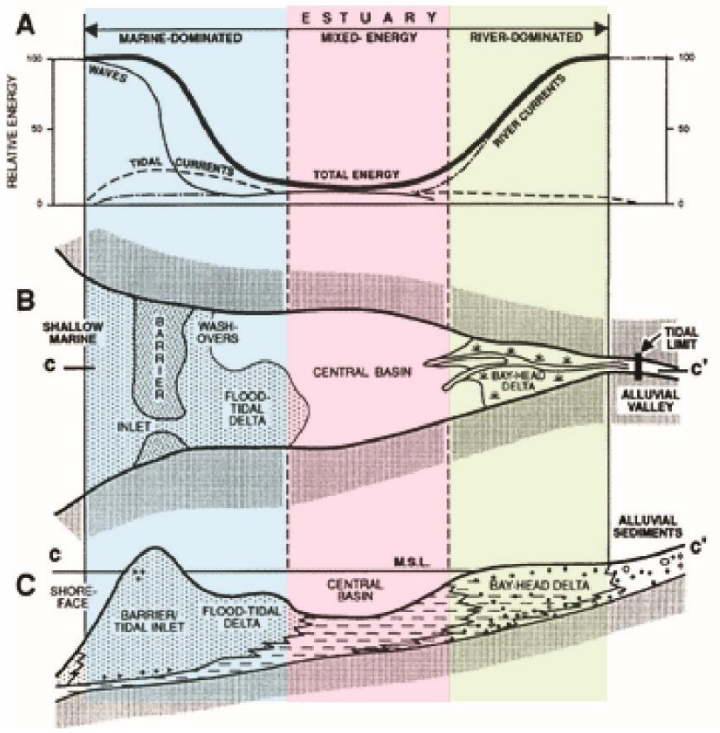

Figure 3. (A) differing energies within the wave-dominated estuarine system. (B) birds eye view of the estuarine system. (C) cross-sectional view of the estuarine system stratigraphy. Figure modified from Dalrymple et al. (1992).

1.2.4 Influence of Weather on Estuaries

Weather conditions are another characteristic that makes estuarine systems dynamic. Estuarine shorelines are subject to rainfall and winds that contribute to elevated water levels and wind-driven waves. These weather events are becoming slow moving with longer impacts due to rise in water temperatures (Phillips, 2022). For example, rainfall, wind-driven waves, and increased storm surges due to Hurricane Florence caused significant damage to both the natural and modified shoreline of the Neuse River Estuary. Storm surges can cause large amounts of saltwater to fill low-lying lands, which causes major flood damage, and in some cases wave action can occur on top of the storm surge (Laird et al., 1975; Phillips, 2022). The increase of wind speeds alone can cause the movement of loose sediments and sands which either block an

estuary from exchange from the ocean to the fluvial component or cause a break in barrier islands. Rainfall due to hurricanes also affects estuaries by eroding inland areas and transporting sediment loads downstream (Laird et al., 1975). Weather conditions are a contributing factor to estuarine shoreline erosion.

1.2.5 Influence of Currents in Estuaries

Another characteristic that defines an estuarine system is currents. Currents are a faster flow of water through a slower-moving body of water. Large-scale currents such as the Gulf Stream and Labrador Current on the east coast impact the water temperature on the coastal shorelines. The Gulf Stream is a warmer current that flows away from the east coast and meets the Labrador Current which is colder water moving south along the east coast. This convergence of currents is where rough seas occur offshore (Laird et al., 1975). Currents are a characteristic of estuarine systems that impact the water temperatures and can cause changes along the shoreline.

1.3 Techniques Used to Monitor Changes in Nearshore Environments

One of the major goals of the National Oceanic and Atmospheric Administration (NOAA) is to update bathymetry data for the world's oceans, as most bathymetric data has not been updated since the 1930s when sound was first used to measure depths (NOAA, 2016). Current bathymetric survey data span from the 1800's to present using a range of technologies from traditional lead line surveys to more advanced multibeam surveys. A straight forward and easy approach, lead line surveys were used in the mid 1800's to measure depths using ropes or lines with measured depth markings attached with a weight at the bottom (NOAA, 2016). A major disadvantage to this approach is that results are sparse in coverage along the seafloor. In the early 1900's, wire drag surveys were used to measure depths and consisted of a weighted wire-drag that was attached between two known locations at a set distance (NOAA, 2016). If the weighted

wire came across something along the seafloor, the wire would create a "V" shape and then a measurement of depth of the obstruction would be measured. This approach would not be advantageous in homogeneous sandy bottoms where there are little to no obstructions to measure depths.

In the 1930's, Dr. Herbert Grove Dorsey of the US Coast and Geodetic Survey introduced the use of sound to measure the depth of the seafloor from the base of a ship, also known as a fathometer which was the first of its kind to record continuous measurements (*The Submarine Signal Fathometer for Visual Echo Soundings*, 1930; NOAA, 2016;). Fathometers were used along a line at set increments to obtain more data, which were more efficient and accurate than the lead line and wire drag surveys (Smith, 1935). More recently, Sound Navigation and Ranging (Sonar) technologies (1950's-Present) have been used. Sonar technologies have been used with many improvements throughout the more recent years. Side-scan sonar is when a vessel drags behind a device to collect sonar images of the seafloor. Single-beam sonar is where the measurements are taken directly below the vessel, generating a single beam of data along the seafloor. Multi-beam sonar is the same idea as a single beam but collects data of the seafloor in a fan motion (NOAA, 2016). The current historical data provided by NOAA is useful, but not for the current real-time changing shorelines and nearshore bathymetry, especially presented in the Neuse River Estuary.

Aside from costly traditional sonar surveys, variations in surveys have been used to collect shallow bathymetric data. For example, airborne laser bathymetry (ALB), which is attached to a plane, uses light detection and ranging (LiDAR) in the blue-green bands of the electromagnetic spectrum to penetrate shallow underwater environments with depths depending on the water clarity and instrument used (Doneus et al., 2015). An advantage to this approach is the ability to

cover vast areas in a timely manner. Satellite-derived bathymetry (SDB) uses multispectral satellite imagery to estimate depths (Muzirafuti et al., 2020). Similarly, depths can be derived from high resolution imagery collected onboard an Unoccupied Aerial Vehicle (UAV) (Matsuba & Sato, 2018). While the advantages to using imagery include accurate nearshore bathymetric estimations that are cost-effective, they use estimation as the key component for data analysis. Additionally, in waters with suspended sediment such as the Neuse River Estuary, the bottom or depth cannot be accurately detected. On the other hand, the more traditional way of sonar attached to a vessel uses actual depth measurements that can detect bottom or depth in murky estuary waters, such as the Neuse River Estuary.

1.4 Objectives

This study aims to collect bathymetric data using new on-demand remote sensing devices such as a small Unoccupied Surface Vessel (sUSV) in attempt to quantify nearshore morphological changes as depositional or erosional volume in the Neuse River Estuary. To achieve this objective, a combination of field and lab experiments are conducted. Two RTK-GNSS and sUSV single-beam sonar surveys are carried out in Spring 2022. The datasets are processed in the lab to create bathymetric models used to calculate volumetric changes between the two surfaces. The surfaces are also compared with topobathy LiDAR collected in 2020 allowing for a two-year assessment of morphological change. The specific objectives of this study are to: 1) generate reliable bathymetric models with acceptable accuracy and precision, 2) using the bathymetric models, assess morphological change as depositional or erosional volume, 3) compare volumetric changes with simultaneously observed wind and wave data to determine any patterns, and 4) create a workflow of best practices when conducting sUSV surveys. It is

anticipated that the results from this study will provide insights into the causes of nearshore morphological change in an estuarine environment.

Chapter 2: Study Area and Data

2.1 Study Area

The study area is located at approximately 34°59'29" N and 76°51'27" W (relative to the World Geodetic System of 1984 or WGS 84) (Figure 4). It is in the Neuse River estuary, which is a drowned river valley, meaning the orientation and underlying geologic features have impacts on sediment dynamics (Benninger & Wells, 1993). The estuary is wide and shallow with sandy areas along the shore. There is a bend roughly 30 kilometers upstream from the mouth, which makes the upper portion (above the bend) orientate northwest-southeast, while the lower portion (below the bend) orientates southwest-northeast (see Figure 4). Therefore, the lower half of the estuary is in orientation with the Pamlico Sound where northeast windstorm events occur and cause major sediment transport and wave actions. The Pamlico Sound has a series of barrier islands known as the Outer banks that prohibit intense tidal interactions. Another important geologic feature that protects the estuary from marine interactions is a bluff shoal found in the bathymetry of the Pamlico Sound. As sea level rises, this bathymetric feature will become less prominent allowing higher storm surges and wave heights to act further up the estuary (Clunies et al., 2017). This indicates that as sea level rises, the estuary could become a marine-based system in the future where sediment transfer moves more marine based materials to the river mouth (Mulligan et al., 2019; Phillips, 2022)

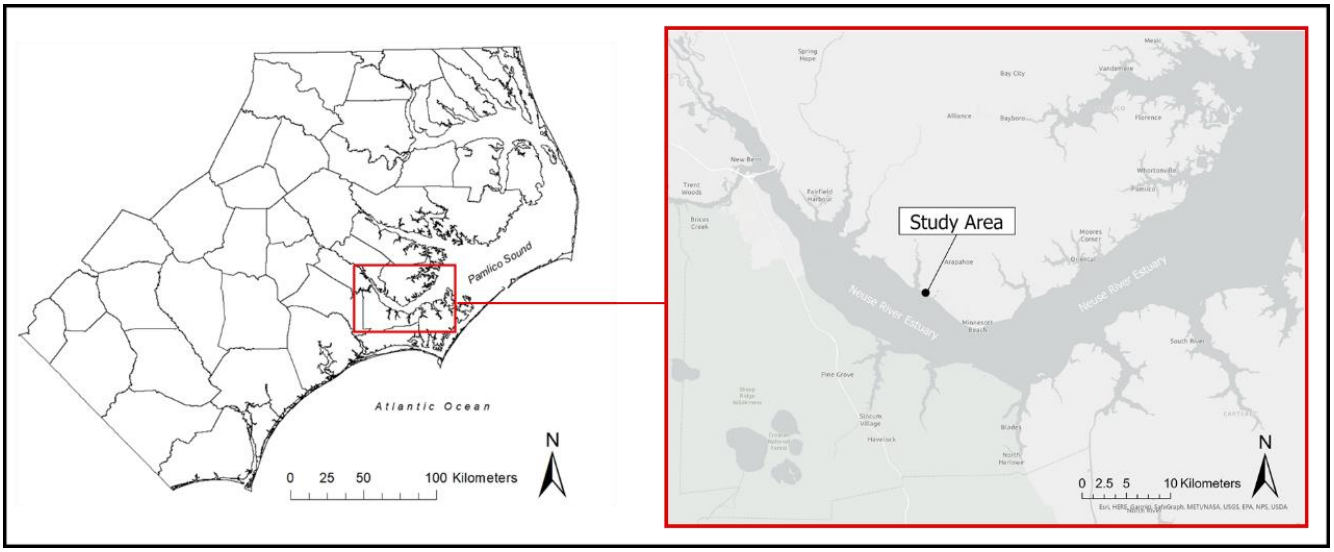

Figure 4. Study site location along the Neuse River Estuary. Study Area: YMCA Camp Seafarer.

2.1.1 Neuse River Estuary Wind and Waves

Since the estuary is microtidal, tidal currents have a minor effect on sediment dynamics within the study area. Instead, it is strong wind events that influence waves and wave-dominated actions that cause major shoreline erosion and thus related nearshore bathymetric changes. Seasonal dominant winds are from the south-southwest in the summer and north-northwest in the winter (Benninger & Wells, 1993). However, the highest average fetch direction comes from the east (Reide Corbett et al., 2008). Hurricanes and northeasters produce winds out of the eastern quadrants and along with the orientation of the Albemarle-Pamlico Estuarine System (APES). The study area is located on the north shore of the estuary and faces in the southwest direction (Figure 4).

2.1.2 Sediment Transport in the Estuary

Studies have been conducted along the estuary to analyze sediment transport. Philips 1992 found that a portion of sediments in the estuary within the Piedmont region or inner zone

does not reach the Coastal Plain region. Therefore, there is little fluvial input for the estuary (Phillips, 2022), so little river-dominant sediment occurs (Benninger & Wells, 1993). It is coastal plain erosion that contributes to a significant source of sediments in the lower estuary. The estuary erodes primarily due to wind-driven waves and other coastal influences in the transition zone and mixing zone (Phillips, 1992). The mouth estuary is predominantly marine sourced. The estuary is situated on the east coast of the United States and therefore experiences tropical storms and hurricanes during hurricane season (June 1st-Novemebr 30th). Therefore, six months out the year the estuary is subject to severe weather that can alter the dynamics of the estuary and its populated shorelines. The estuary was hardest hit by Hurricane Florence in September 2018, which caused inland flooding from precipitation and storm surge from the ocean leading to bluff retreat as much as 11 m (Phillips, 2022). As severe weather impacts the estuary and causes changes from the fluvial and marine inputs, it also impacts the shorelines. Estuarine processes impact the sediment budget of nearby shorelines (Hibma et al., 2004). As nearshore bathymetry and shoreline morphology can influence estuarine shoreline changes (Eulie et al., 2017), it is important to measure bathymetry to see the sediment flux.

2.2 Data

2.2.1 Bathymetric LiDAR Data

Public sources of bathymetric data are limited, and this poses a problem when monitoring present changes of estuarine bathymetry on smaller scale locations in a select area of interest. For the first time, a LiDAR topobathy survey has been conducted in the estuary which can be compared with the data collected in this study to assess any morphological changes between them. The NOAA Florence Topobathy LiDAR data were collected by NV5 Geospatial in spring 2020 using a Riegl VQ880GII sensor with a green and infrared laser scanner. In turbid areas,

fewer pulses may have penetrated the water surface, resulting in lower bathymetric density. The density of bathymetry points is reported on average > 2 pts per m^2, but fewer pulses may have penetrated the surface in turbid areas. The vendor classified the points as bathymetric bottom which were interpolated into 1 m resolution bathymetry model. The vender tested the bathymetry model with independent RTK-GNSS points taken in depths up to 1 m where a RMSE of 0.074 m is reported. The data were obtained from: https://coast.noaa.gov/dataviewer.

2.2.2 RTK-GNSS and sUSV surveys

Prior to conducting the sUSV surveys, a benchmark was created in this study using the Trimble Spectra Precision SP80 system with a reported high-precision static post-processed precision of 3 mm in the horizontal and 3.5 mm in the vertical (root mean square error (RMSE) (Trimble, 2019). The +240 channels dual frequency SP80 receiver was used with full utilization of signals from all 6 GNSSs (GPS, GLONASS, BeiDou, Galileo, QZSS, and SBAS) while collecting data at 1-s intervals continuously for a minimum of 4 h. The receiver's raw file was then automatically adjusted with NOAA's Online Positioning User Service (OPUS) solution using Trimble Business Center v5.10 with an overall benchmark RMSE of 0.012 (Table 1).

Table 1. Online Positioning User Service (OPUS) solution for the established benchmark at the study area, YMCA Camp Seafarer.

NAD83 2011 (EPOCH: 2010)	RMSE	State Plane Coordinates: SPC (3200 NC)
N 34°59' 48.46945"	0.006 (m)	Northing: 140,419.332 (m)
W 76° 51' 24.02352"	0.002 (m)	Easting: 805,231.021 (m)
Ellipsoid Height: -36.250 (m)	0.002 (m)	
Orthometric Height: 1.190 (m)		
[NAVD88 using GEOID 18]	0.053 (m)	
Overall	0.012 (m)	

Two RTK-GNSS receivers were used in the sUSV surveys where one was set-up as a base station placed over the benchmark and the other was mounted on a Seafloor Systems Echoboat-

160 sUSVz (see Table 2 for specifications), which was configured for this study with the Seafloor Systems HydroLite-TM single beam sonar. The HydroLite-TM has a frequency of 200 KHz, beam width of 9 degrees, ping rate of 6 Hz, operating range of 0.3 – 75 m, and reported depth accuracy of 0.01 m (Seafloor Systems Incorporated, 2022). The draft measurement, or distance from where the water level/water line of the water is located to the top of the transducer was measured as 0.36 meters for both surveys (Figure 5, E). Once configured and launched in the water, the sUSV was maneuvered manually using a remote control like Specht et al. (2020). The sUSV survey path was a random cross-hatch pattern (Figure 6) to increase the point overlap, which was subject to change due to wave interaction, current direction, wind interface, etc.

Table 2. Specifications for the Seafloor Systems EchoBoat-160 model used in this study (modified from Seafloor, 2020a).

sUSV Specifications	Description
Typical survey speed	3 kts
Top survey speed	5 kts (payload dependent)
Hull length	1.68 m
Hull width	0.8 m
Hull weight (no batteries or payload)	45 kg/100 lbs
Payload	29 kg/65lbs
Motor	2x Brushless DC Outdrive
Remote control	2.4 GHZ/900 MHz Long Range RCU
Remote Range	Up to 2 km
Communication	2.4 GHz UHF Telemetry

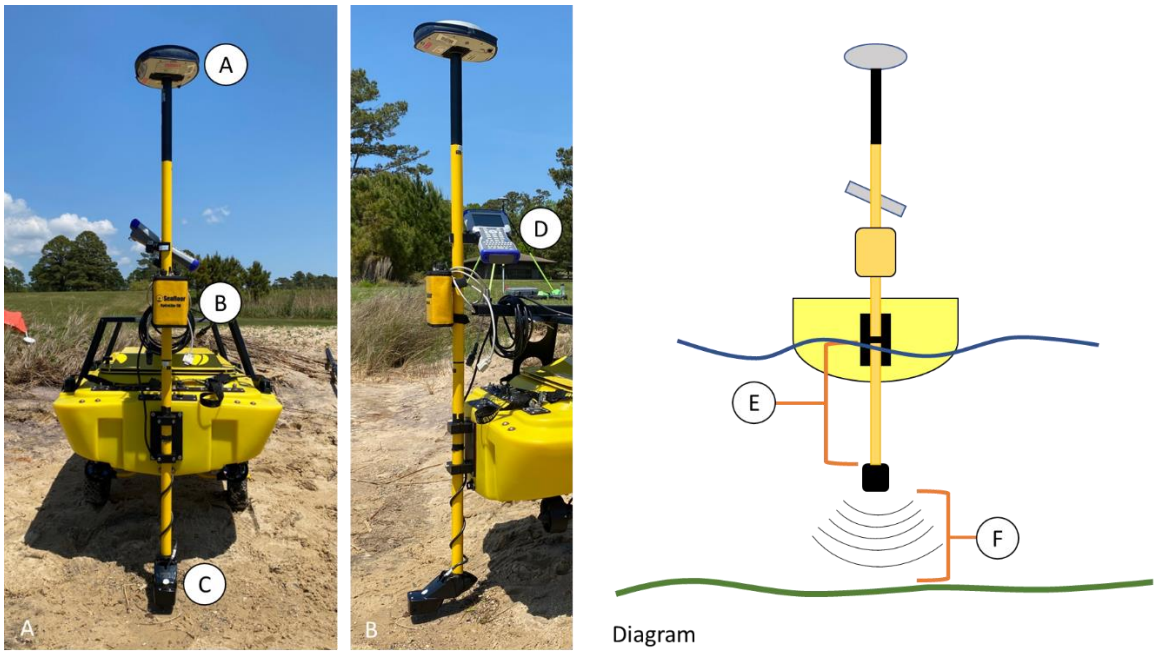

Figure 5. Attachment of the RTK-GNSS unit (A), echosounder (B), transducer (C), and data collector (D) to the stern of the sUSV. The diagram on the right shows the draft measurement (E) where the blue line represents the water line and the green line represents the bed topography. This determines how the sUSV sits on the water and can vary. The depth measurement, Dz (F), is the measurement from the transducer to the bed topography.

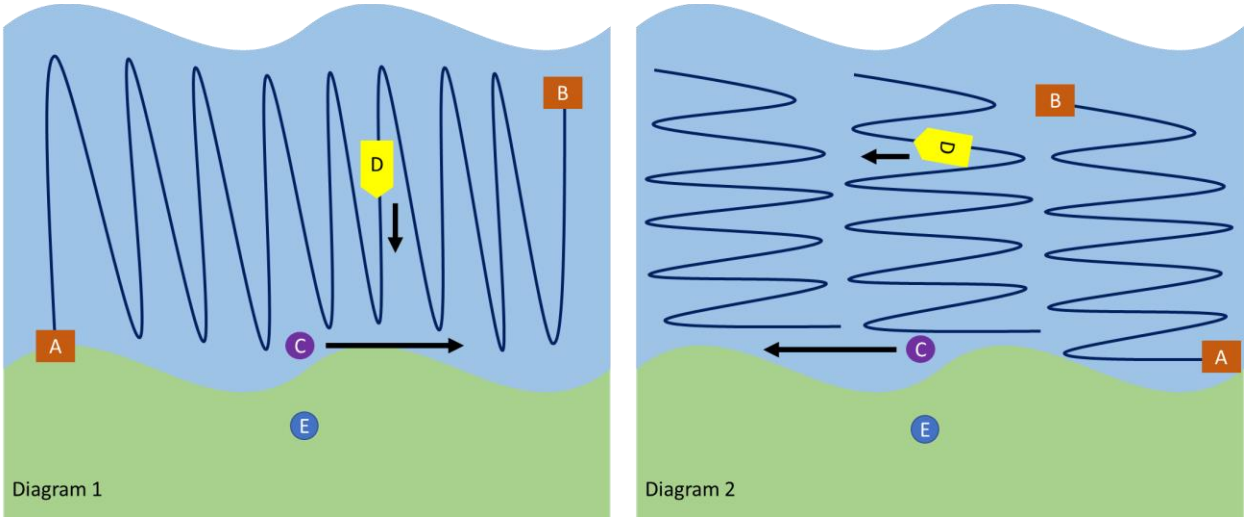

Figure 6. The cross-hatch method used when conducting bathymetric surveys, where A = starting point, B = ending point, C = person in control of the sUSV, D = the sUSV, E = base station location, and the arrows indicate the direction in which C or D are

moving within the survey. The green mass is land and the blue mass is the nearshore waters. Diagram 1 (left) shows the sUSV being maneuvered perpendicular to shore from point A to point B and the person in control is moving to the right while controlling the sUSV. Diagram 2 (right) shows the sUSV being maneuvered parallel to shore from point A to point B (repeating) until the survey is complete and the person in control is moving to the left as the survey continues.

Atmospheric and marine conditions can impact the quality and safety of the sUSV surveys. Prior to and during operation of the sUSV, the aerodrome forecast (TAF) from the National Weather Service (NWS) Aviation Weather Center at www.aviationweather.gov, the Marine Zone Forecast from the NWS at https://www.weather.gov/marine/, and the Marine Weather and Tides for Havelock, NC Havelock, NC Marine Weather and Tide Forecast (l-36.com) were used to analyze the weather. The first survey was conducted on 15 February 2022 with northeast winds of 10 kts, seas 0.6 to 1.2 m, dominant period 5 seconds, waves light chop, visibility > 6 km, and temperatures between 8 and 10°C. The second survey was conducted on 23 April 2022 with northeast winds 5 to 10 kts, seas 0.61 to 0.91 m, dominant period 8 seconds, waves light chop, visibility > 6 km, and temperatures between 18 and 26 °C.

Once a bathymetric survey was completed, a nearshore survey was conducted using a second RTK-GNSS receiver. A topo shoe was equipped on the survey rod allowing the instrumentation to sit on the surface of the bed topography. The RTK-GNSS rover was positioned level with the bed surface at 60 – 180 epochs to record each x,y,z location in waters < 1 m depth. A step-point intercept sampling method was used to collect the RTK-GNSS locations creating transects that included sampling bias from maneuvering through the water. The RTK-GNSS locations were used to assess the accuracy of the bathymetry models generated in this study.

2.2.3 Wind and Wave Data

Wind driven waves are expected to be the primary contributors to nearshore bathymetric change. Therefore, wind and wave sensors were installed at the study site to be paired with each bathymetric survey to detect any related changes. The MetOne Instruments 034B Wind Sensor combines wind speed measurements in the range of 0-167 mph (0-75 m/s) and accuracy of 0.25 mph (0.1 m/s) and wind direction measurements in the mechanical range of 0-360 degrees with an accuracy of ±4 degrees (Met One Instruments, 2001). The wind sensor setup is shown in Figure 7. Water level and wave observations of significant wave heights (Hs) and peak wave periods (Tp) were collected using an Ocean Sensor Systems capacitance wave sensor that samples a frequency of 30 Hz. Each sensor was programmed to sample every 5 s with data stored as 6-min averages.

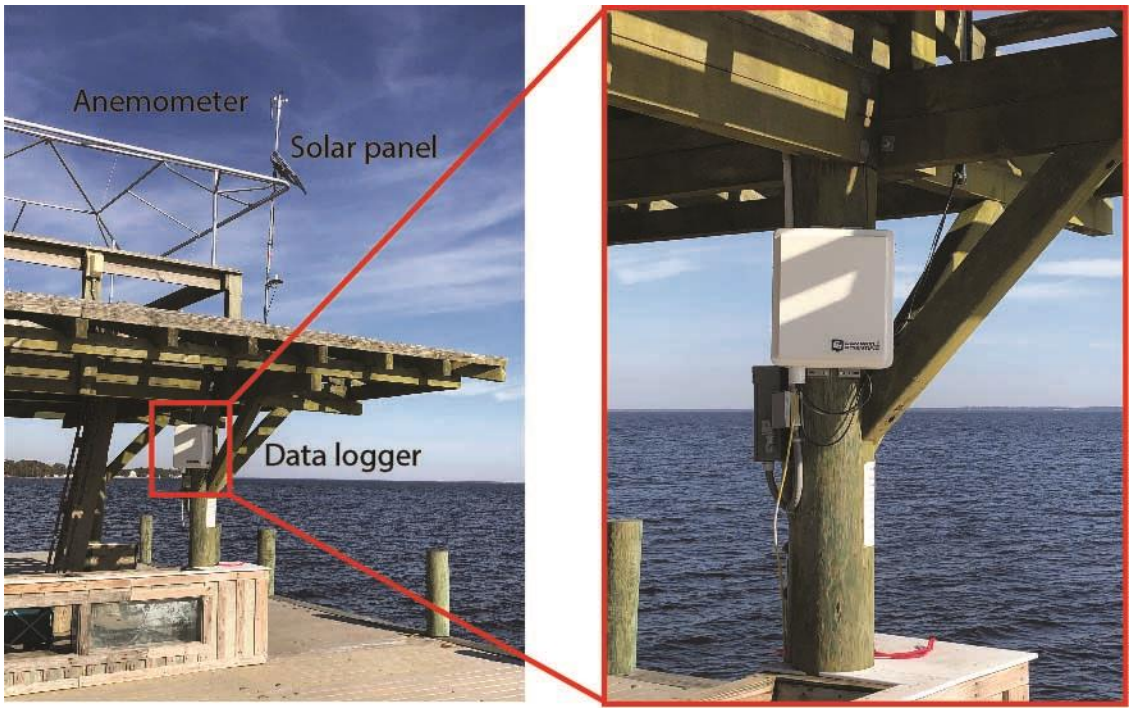

Figure 7. MetOne Instruments 034B Wind Sensor setup at the end of a dock at YMCA Camp Sea Gull located on the north shore of the Neuse River estuary, which is the study area.

Chapter 3: Methodology

An overview of the methods used to create bathymetric models is provided. First, the RTK-GNSS and corresponding sonar data were used to calculate values for bed topography and water depth. These data were then examined by the point density to determine the minimum horizontal resolution. Three interpolation techniques were used to generate three surfaces for each of the two surveys with the same horizontal resolution and cell alignment. An accuracy assessment was performed on each of the three bathymetry models by calculating the difference between independent RTK-GNSS values and the interpolated surface values. The resulting bathymetric models that had the best accuracy were used to assess any changes that may be related with the wind and wave data.

3.1 Bathymetry Calculations

The bathymetry, or underwater elevation relative to a vertical datum, is important for understanding nearshore morphological changes. In this study, Trimble Business Center (TBC) was used to correct the RTK-GNSS *x,y* locations for each pulse sounding. At this point, the attributes included the northing and easting measurements, elevation relative to NAVD88 (using Geoid 18), error in the horizontal and vertical, and transducer depth measurement. Since we are interested in bathymetry, a field was added to the attribute table. The bathymetry field was calculated using the following (Equation 1):

$$Elevation - Dz = Bathymetry \qquad (Equation\ 1)$$

where *Elevation* = RTK-GNSS elevation relative to NAVD88, *Dz* = the transducer depth measurement, and *Bathymetry* = bed elevation relative to NAVD88. The result is a point file

where each *x,y* location has an elevation value relative to NAVD 88 that can be interpolated to create a continuous surface.

3.2 Bathymetric Model Generation

Before interpolating a surface from points, the point density, average point spacing, and cell size of the bathymetric model needs to be determined. The overall point density is the amount of measurements for a surveyed area (Felix Rohrbach, 2015) and was calculated using the following formula from Vallé & Pasternack, 2006:

$$Overall\ Point\ Density = \frac{\Sigma\ Points}{Survey\ Area} \qquad (Equation\ 2)$$

This study used a specific cell size (see later) unique to each survey completed. ArcGIS Pro was used to calculate the average point spacing for the specific output raster used for each survey. The Point Density (Geostatistical Analyst Tool) in ArcGIS Pro was used where the input points field were populated by each survey, the cell size was determined and inserted, and a mask was populated for the survey area to obtain the average, or mean, point density for the specified cell size.

Point spacing is the distance between two points (Felix Rohrbach, 2015) and was calculated using the following formula:

$$Point\ Spacing = \sqrt{\frac{1}{Point\ Density}} \qquad (Equation\ 3)$$

Equation 3 was modified from Felix Rohrbach (2015) to utilize the specific cell size generated from the surveys. The point density parameter used the average point density determined by the Point Density (Geostatistical Analyst Tool) in ArcGIS Pro, as the values were specific to the cell size for the February and April surveys.

Hu (2003) introduced a mathematical approach to calculating cell size using the following formula:

$$Cell\ size = \sqrt{\frac{Area}{Number\ of\ Points}} \qquad (Equation\ 4)$$

Equation 4 was adopted in this study to calculate cell size. To calculate the cell size, the area must be known. Just like matching cell sizes, the area must be the same for both datasets. In this study, a polygon layer was created around the bulk of the point data (the April survey was used because it covered slightly less area). This same polygon was then used to select all points that fell within the polygon area to create a new dataset for both surveys. This allows for consistent interpolation boundaries as well as cell size calculation. Once the area was determined, the number of points from each survey that fell within the polygon were calculated. The data with the largest cell size will be used to determine the horizontal resolution for all interpolated bathymetry models so their cell sizes match.

Single-beam sonar measures a single point measurement directly below the transducer, which means there will naturally be gaps within the survey transects. To fill the gaps, this study uses spatial interpolation, which is a process of using the points of known values to estimate the points of unknown values. Spatial interpolation can be done by various techniques such as Empirical Bayesian Kriging (EBK), Global Polynomial Interpolation (GPI), or Spline. EBK is popular because it is an automated geostatistical interpolation method that makes reliable estimations (Krivoruchko and Gribov, 2014). GPI uses a mathematical polynomial function to calculate a surface that represents gradual trends (esri, n.d.). Spline also uses a mathematical function, which minimizes surface curvature (Franke, 1982). Each interpolator has unique

characteristics. EBK is both an exact (original data values stay the same) and inexact interpolator (new estimates replace original data values). GPI is an inexact interpolator where new estimates replace original data values. On the other hand, Spline is an exact interpolator where original data values stay the same. Due to their unique characteristics, each interpolation produces a unique surface, so each will be tested in this study to determine which provides a more reliable estimation of the true bathymetry.

With the cell size determined and interpolators chosen, the point data were interpolated in this study using ArcGIS Pro. EBK interpolator, which is the Empirical Bayesian Kriging (Geostatistical Analyst Tools) in ArcGIS Pro, was used with all parameters set at default to generate a prediction surface at the specified cell size. GPI interpolator, or Global Polynomial Interpolation (Geostatistical Analyst Tools) in ArcGIS Pro, was used with a polynomial order of one because there are few bends in the nearshore bathymetry at the study site. The same cell size was specified, but this time environments were changed where Snap Raster option was populated with the bathymetry model created from EBK. This results in a bathymetry surface created from GPI that has the same cell size and alignment as the bathymetry surface created from EBK. Spline interpolation, or Spline (Spatial Analyst Tool) in ArcGIS Pro was used with the spline type of regularized and default weight of 0.1 and number of points of 12. Once again, the Snap Raster setting was populated. The results for each the February and April datasets are an EBK, GPI and Spline-generated bathymetric model, or 6 total (2 dates x 3 interpolators = 6 datasets).

3.3 Bathymetric Model Accuracy Assessment

The accuracy of the interpolated BEMs was assessed using independent RTK-GNSS points collected in the field. The bathymetric model's grid cell values were extracted to the RTK-GNSS points using the Extract Values to Points (Spatial Analyst) in ArcGIS Pro. A new column was

added to the attribute table, and the difference between the grid cell value and RTK-GNSS value was calculated (RTK-GNSS – grid cell value = difference). Summary statistics such as mean bias error and standard deviation were calculated. The vertical RMSE was also calculated using the following equation:

$$RMSE = \sqrt{\frac{\Sigma_{i=1}^{n}(BEM_i - GNSS_i)^2}{n}} \qquad (Equation\ 5)$$

where BEM_i = the Bathymetric Elevation Model (BEM) grid cell value, $GNSS_i$ = the RTK-GNSS point value, n = the number of matched test data samples, and i = an integer from 1 to n. The results are a table of descriptive statistics on the 3 interpolators' performance.

3.4 Change Detection

Once the bathymetric models are generated, the differences between them can be calculated to create a BEM of difference (BoD) (see Wheaton et al. 2010). A BoD was created in this study using Raster Calculator (Spatial Analyst Tool) in ArcGIS Pro with the following (Equation 5):

$$BEM_1 - BEM_2 = change \qquad (Equation\ 6)$$

where BEM_1 = the new bathymetric model (example: April 2022), BEM_2 = the old bathymetric model (example: February 2022), and *change* = a positive value of sediment gain or a negative value of sediment loss. Before volumetric change could be analyzed, each BEM's mean bias error was eliminated to properly compare each survey. Raster calculator was used to eliminate the mean bias error using the following equation:

$$BEM - Mean\ Bias\ Error = BEM_c \qquad (Equation\ 7)$$

where *BEM* = the bathymetry model derived from the ideal interpolation technique chosen from the results, *Mean Bias Error* = Mean bias error specific to that BEM, and BEM_c = BEM corrected by the mean bias error ready for volumetric change detection.

Volumetric change was then determined in Raster Calculator by multiplying the change in elevation in each grid cell by the surface area of each grid cell using the following equation:

$$(BEM_{c1} - BEM_{c2}) * cell\ size^2 = volumetric\ change \quad (Equation\ 8)$$

where BEM_{c1} = new bathymetric model corrected by the mean bias error, BEM_{c2} = old bathymetric model corrected by the mean bias error, *cell size* = the determined grid cell size used, and *volumetric change* = a positive value of sediment gain or a negative value of sediment loss. The results were a DoD, volumetric change raster, and total deposition and erosion.

Chapter 4: Results and Discussion

4.1 Bathymetry Maps

The overall point density was determined for February as 0.122 points per square meter, and 0.129 points per square meter for April. The average point density for February was 388 points per 3 square meters, and April 353 points per 3 square meters. The point spacing for February was 0.051 and April was 0.053. Point density and point spacing for each survey (Table 3) was generated resulting in a sparse point cloud with 0.051 points per 3 square meters for the February survey, and 0.053 points per 3 square meters for the April survey.

The cell size used when generating the BEMs was determined by taking the square root of the survey area divided by the number of survey points that fell within that area (Table 4, Figure 8). The February survey resulted in a slightly larger cell size when compared to the April survey (Table 3). For a conservative estimate, this study used a cell size of 3 m to generate the BEMs. For each the February and April survey datasets, three BEMs were generated from the sUSV survey points using EBK, GPI, and Spline interpolators (see Figure 8 showing the sUSV survey points). In the maps, lighter shades of green indicate lower elevations while darker shades of green indicate higher elevations (Figure 9). Based on actual observations made in the field, a visual examination of each interpolator's results can be assessed. While the nearshore bed topography had a gradual slope, the GPI maps appear unnatural with only two elevation breaks. This is due to the first order polynomial that is fitted to all the data values at once, which seemed reasonable at first given few bends in the nearshore bathymetry. The Spline maps also show some discrepancies from what was observed in the field such as elevations closest to the shoreline that are >-0.59 m (lighter greens) and then drop <-0.99 m (darker greens). This is likely due to the Spline interpolation fitting low-degree polynomials to small subsets of the data. On the

other hand, a visual examination of the EBK maps show gradual undulations in the bed topography, which more closely align with what was observed in the field. After a visual examination of each interpolator's results, EBK seems to estimate the nearshore bathymetry better than GPI and Spline.

Table 3. Point density and point spacing for the February 2022 and April 2022 surveys.

Survey	Overall Point Density (Points/Square M)	Average Point Density (Points/ 3 Square M)	Point Spacing
February	0.122	388	0.051
April	0.129	353	0.053

Table 4. Parameters used to calculate the minimum cell size based on the area and number of survey points that fell within that area. The cell size used for investigation was 3 m.

Survey Date	Survey Area (Square M)	Number of Survey Points	Cell Size
15-Feb-22	18,535	2,262	2.86
23-Apr-22	18,535	2,394	2.78

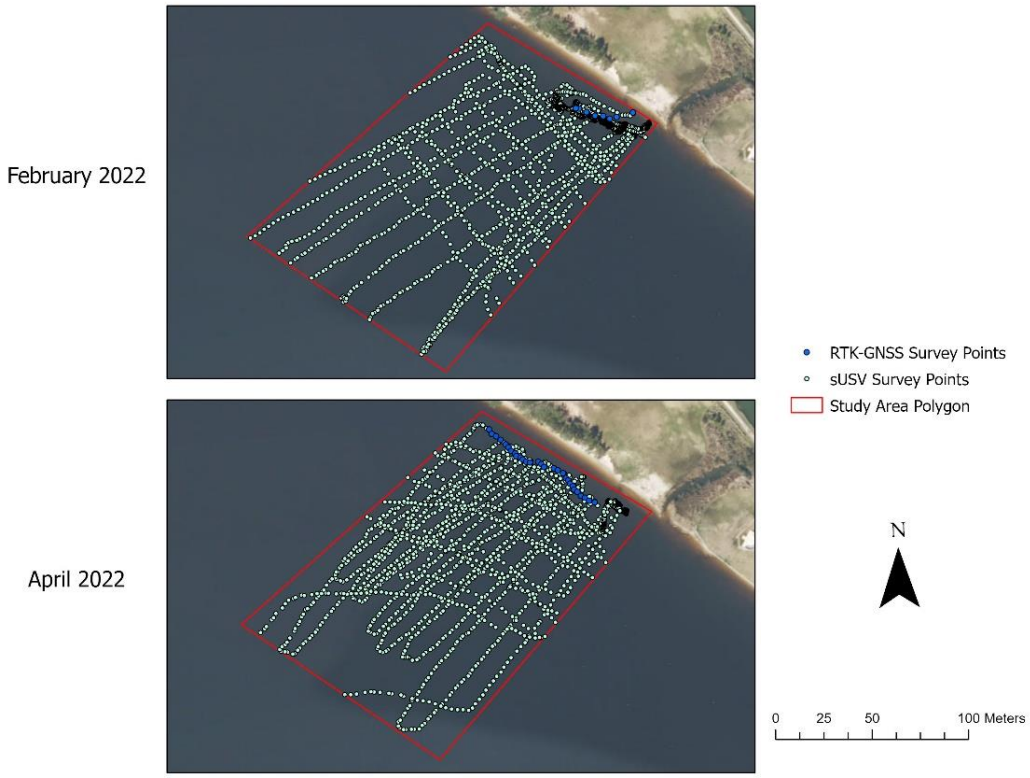

Figure 8: February and April surveys showing RTK-GNSS and sUSV survey points within the study area polygon.

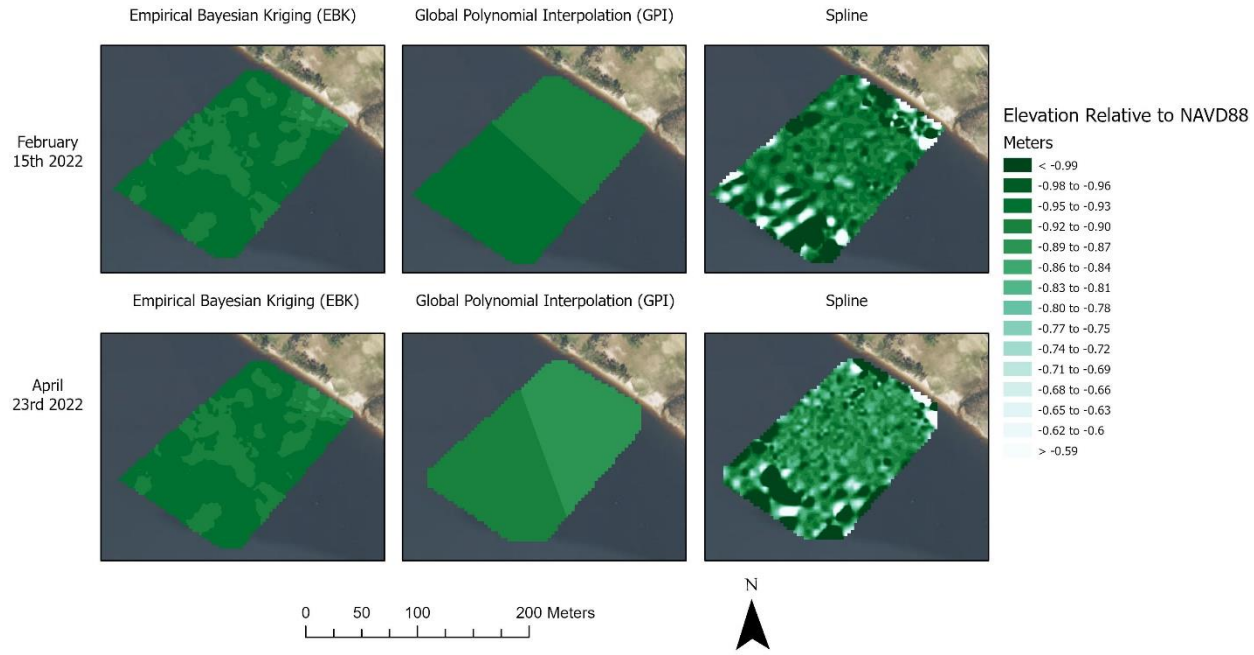

Figure 9. BEMs of the Bed Topography for the February and April surveys.

4.2 Bathymetric Model Accuracy

Descriptive statistics of each bathymetry model were calculated using the differences, or errors, between the independent RTK-GNSS points and the interpolated grid cell value at the same location (RTK-GNSS – grid cell value = difference). Table 5 shows the mean bias error, standard deviation, and RMSE of each interpolation approach tested in this study. The mean bias error is an average of all the errors, which is an estimate of how much the interpolated values over- or underestimate the true surface. All experiments contained a positive bias meaning all interpolators overestimated the surface. The standard deviation of the errors was calculated, which is a measure of precision that represents the errors around the mean. The February experiments contained a small range of standard deviations (0.04 m), while the April surveys contained a large range of 0.17 m. The reason for this may be due to the number of RTK-GNSS

points that are much lower for the February survey when compared to the April survey, but this needs to be tested. The differences between the summary statistics for the February experiments are not significantly different, and since the EBK provided a better visual representation of the nearshore bathymetry, it was chosen for further analysis. For the April survey, the EBK was chosen because it had the lowest standard deviation and RMSE, and it provided a better visual presentation of the nearshore bathymetry.

Table 5. Bathymetric model accuracy by interpolation experiment. Where n = the number of RTK-GNSS points, units are in meters.

Experiment	n	Mean Bias Error	Standard Deviation Error	Vertical Root Mean Square Error
EBK February	**9**	**0.05**	**0.22**	**0.21**
GPI February	9	0.03	0.22	0.21
Spline February	9	0.04	0.26	0.25
EBK April	**29**	**0.15**	**0.04**	**0.15**
GPI April	29	0.15	0.04	0.16
Spline April	29	0.11	0.21	0.23

4.3 Wind and Wave Characteristics

Wind measurements were collected from the MetOne Instruments 034B Wind Sensor located at the study site for the survey months of February and April 2022. Every minute there were six wind speed and wind direction measurements, respectively. From these measurements, the hourly average wind speed and hourly average wind direction were calculated. These condensed measurements were then graphed to analyze the general direction and speed for each month (Figure 10). Both months showed wind speeds no higher than 18 meters per second. Wind speeds were then grouped into three segments, 0-5 m/s, 5-10 m/s, and >10 m/s. February shows

dominant wind speeds of 5-10 m/s in the Northeast and South directions (Figure 9-A), while April shows dominant wind speeds of 5-10 m/s in the Southwest direction (Figure 9-B). Therefore, both months show majority of the wind speeds being within the 5-10 m/s segment while having different directions. This trend compares with Benninger & Wells (1993) as seasonal dominant winds are from the south-southwest in the summer and north-northwest in the winter. For comparison with our measurements, New Bern, NC wind data [New Bern, NC Weather History | Weather Underground (wunderground.com)] showed a slightly lower average of ~3.3 m/s for February 2022 and ~3.4 m/s for April 2022.

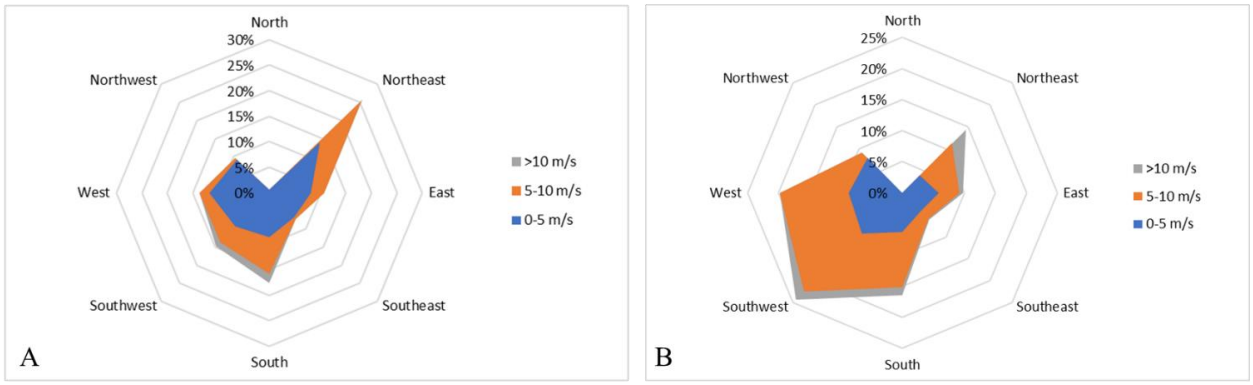

Figure 10. Average wind speed and direction for February (A) and April (B) at Camp Seagull.

Water level and wave observations of significant wave heights were collected at the study site using an Ocean Sensor Systems capacitance wave sensor. Every second, the wave sensor recorded three measurements of the wave depth maximum wave depth minimum, and the wave standard deviation. This resulted in 177 measurements for one minute of instrument recording and 254,880 measurements per day. In this study, the wave data was averaged for each day and month to get an average wave depth maximum, wave depth minimum, and wave depth standard deviation for both February and April (Table 6). As can be expected in a wave dominated estuary

where both months had wind speeds within the 5-10 m/s, wave depth minimum and maximum ranges are small. The wave depth minimum and maximum ranges just 0.01 cm for February and 0.01 cm for April. The 90th percentile was also calculated for both February and April (Figure 11) displaying 90 percent of the wave height maximum and minimum data for each month. There is a general increase in wave height maximums and minimums for both February and April, where some days show smaller wave heights than the general increase. The difference between the maximum and minimum was 0.05 m for February and 0.03 m for April.

Table 6. Average monthly wave maximum and minimum depths for February and April.

Month	Depth Max (m)	Depth Min (m)	Depth Std (m)
February	0.571	0.570	0.009
April	0.642	0.641	0.012

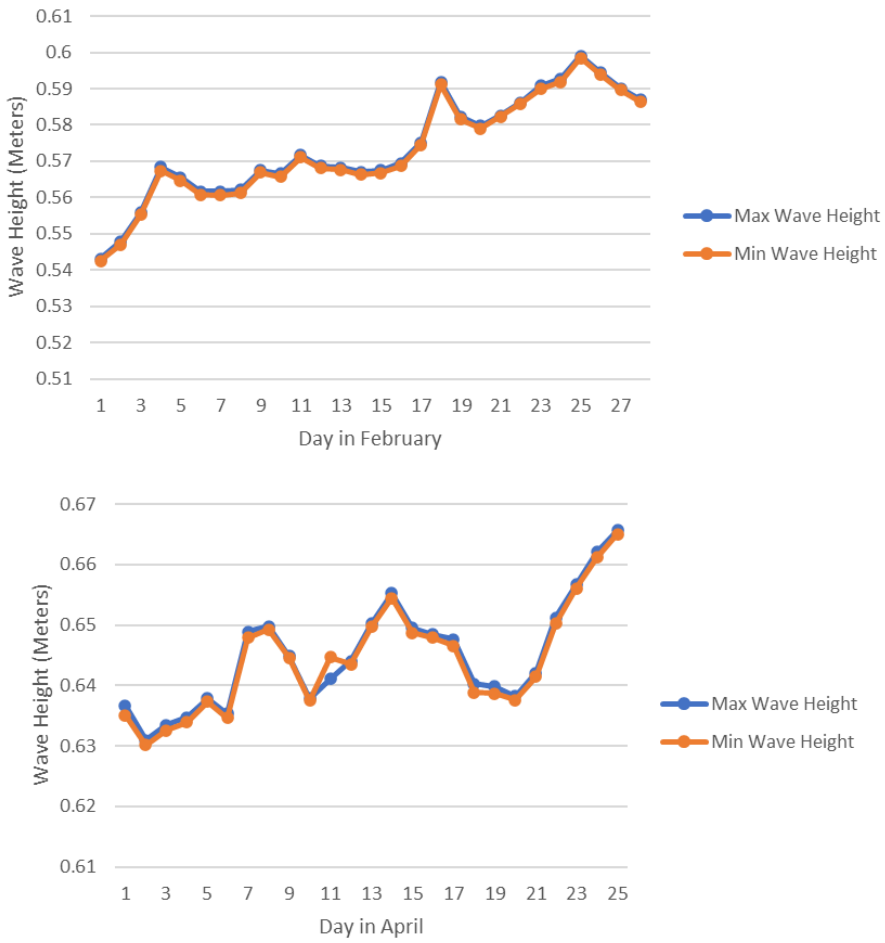

Figure 11. 90th Percentile wave heights for February and April.

4.4 Observed Morphological Changes

Morphological changes were observed in this study as long-term volumetric changes (the difference between LiDAR 2020 BEM and February 2022 BEM multiplied by the area of the grid cell, and LiDAR 2020 BEM and April 2022 BEM multiplied by the area of the grid cell), and short-term volumetric changes (the difference between February 2022 BEM and April 2022 BEM multiplied by the area of the grid cell). It is important to note that since the February and April 20222 BEMs had their mean bias corrected to zero, and the February 2022 BEM had the largest RMSE of 0.21 m (see Table 4), all changes ±0.21 m were eliminated from the analysis

where the minimum change detection value was 0.22 m (see the legend in Figures 12 and 13). Changes in the nearshore bathymetry for the long-term are all negative meaning the February 2022 BEM is lower than the LiDAR 2020 BEM, and the April 2022 BEM is lower than the LiDAR 2020 BEM (Figure 12). Therefore, the results are erosional and not depositional values for the long-term volumetric changes. Historical monthly events were investigated at Climate Data Online (CDO) - The National Climatic Data Center's (NCDC) Climate Data Online (CDO) provides free access to NCDC's archive of historical weather and climate data in addition to station history information. | National Climatic Data Center (NCDC) (noaa.gov) for the timeframe 2020 through April 2022. No specific weather events caused interest for direct changes along the Neuse River Estuary. The short-term changes are also negative meaning the April 2022 BEM is lower than the February 2022 BEM continuing the trend of erosion in the nearshore bathymetry. In the map, lighter shades of green indicate less erosion while darker shades of green indicate more erosion (Figure 13). It is interesting the results show grid cells with losses less than 1 m (darker shades in Figure 13).

As there were no direct historical weather events that could cause such erosion in the estuary nearshore, and wind and wave events were not strong influencers in the estuary during this time, it is expected more intense events such as hurricanes cause changes along the shoreline bluffs and nearshore interaction. Hurricane Florence occurred in 2018 and caused erosional changes to the estuary shoreline, as storm surge occurred, and wave actions occurred on top of the storm surge causing erosion of the bluff shorelines. Sediments that were eroded in 2018 on the shoreline bluffs could have been moved to the nearshore in a mass amount and since there has not been a significant hurricane or tropical storm to impact the NRE since Hurricane Florence, it could be the sediment from Florence is slowly moving from the nearshore to the deeper portions

of the estuary, without shoreline bluff sediments impacting the nearshore. This could cause a steady removal of sediments from the nearshore with little influence from the shoreline bluff sediments. This is difficult to determine as there were no wind and wave sensors during this time to justify this further. Another influence for erosion in the nearshore could be currents, where sediments could travel throughout the estuary with a current flow acting within the estuary, removing excess nearshore sediments from a major hurricane event, such as Florence. Also, the orientation of the NRE could impact the erosional aspects of the nearshore and the bluff shoreline features. Portions of the estuary are in line with the Albemarle-Pamlico Sound which cause certain areas along the NRE to be exposed to more direct influences from Sound parameters. There could be more erosion in the higher risk areas that line up with the orientation of the Sound. Other areas of the NRE could be shielded from the direct influences of the Sound due to orientation and could cause less erosion along the bluff shorelines and more erosion within the nearshore, due to currents for example.

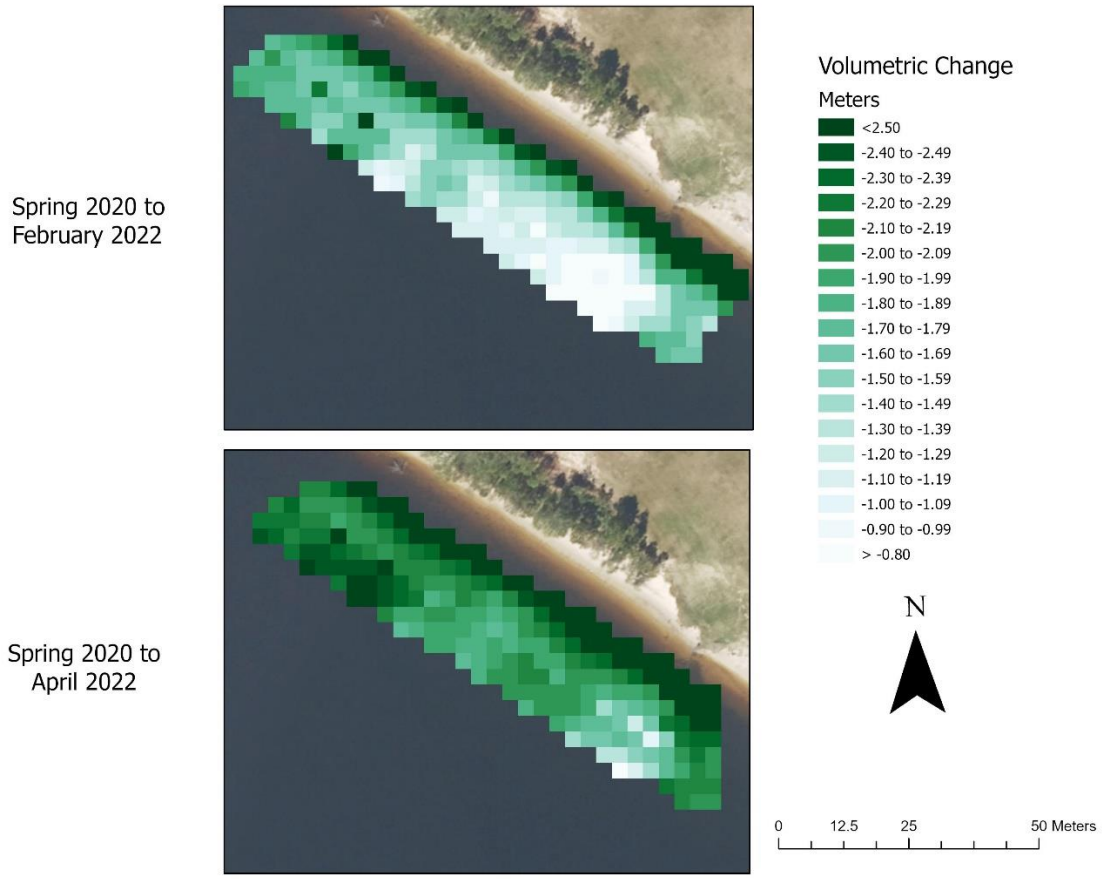

Figure 12. Long term bed topography changes between the LiDAR 2020 BEM and February 2022 BEM, and LiDAR 2020 BEM and April 2022 BEM.

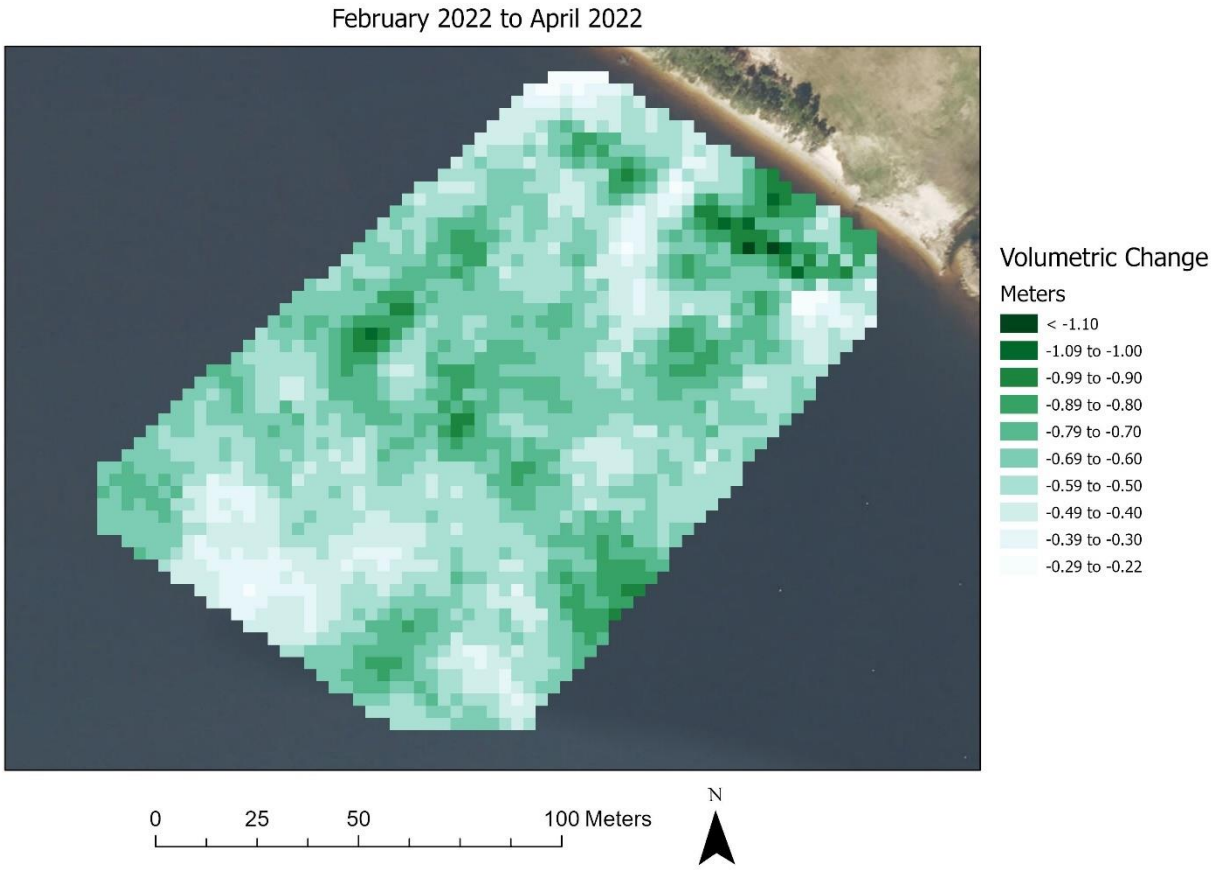

Figure 13. Short term bed topography changes between the February and April 2022 BEM.

4.5 Challenges to Using sUSV in Nearshore Estuarine Environments

The sUSV is a new tool to use in low energy wave environments that can aid in bathymetric surveys, but there are limitations while using this equipment. When selecting a survey area site, it is important to acknowledge the type of shoreline topography and nearshore bathymetry features. The SBES used in this study needed a minimum of 30 cm to begin collecting depth soundings. This means that the sUSV might need to be carried or transported in the water for up to 0.6 m to acquire the desired depth for a survey to collect data and not damage the equipment (Figure 14A). A team of at least two to three people are needed for each survey (Figure 14B). If

there is not a designated field team, this can be challenging to acquire the amount of people required to help as the sUSV used in this study weighed 45kg/100lbs without any equipment added and the length is 1.68 m. The transportation of the sUSV to each survey required a large truck bed. If there is not a large vehicle or trailer available for transportation, this can limit the range of survey sites. Some survey sites might have steep bluff shoreline features with pine trees on the top portion of the bluff feature (Figure 14C). This can cause an RTK-GNSS error, or a multipath error, which can be from interference of objects such as buildings or dense forested areas. In areas with possible errors, it is possible the RTK-GNSS unit does not connect to the same satellites as the rover unit, and this can cause an error of Differential Global Positioning Systems (DGPS). Once the units are connected, this may take some time where a "FIXED" symbol will appear meaning the RTK-GNSS base and rover units are connected to the same number of satellites. sUSV surveys also require specific boating conditions and weather parameters in order to conduct a survey. The ideal boating conditions include no to low wave chop and wind speeds 0-5 kts (Figure 14D). If the wave and wind conditions are greater than this segment, the sUSV has the potential to capsize. The weather conditions need to be sunny or partly cloudy with no fog for visibility, and the equipment cannot be operated during rain or thunderstorms.

Figure 14. Challenges while using the sUSV in shallow nearshore bathymetric environments. A: Shows the use of three crew members transporting the sUSV through the shallow water. Two crew members to stabilize the sUSV and move the kayak, and one to balance the weight on the kayak. B: Two crew members carrying the sUSV into the water. C: A survey location where the shoreline bluffs of 15 m in elevations and pine tree cover caused RTK-GNSS error. The red circle shows the location of the base station. D: Ideal wave conditions, waves light chop and winds <10 kts, at YMCA Camp Seafarer.

4.6 Best Practices in sUSV surveys

The responsibility of reproducible research experiments is crucial as more scientists across many disciplines find themselves unable to recreate other scientific works (Aarts et al., 2015). A best practices step-by-step survey guide was created in this study to integrate previous sUSV survey techniques and generate proper field techniques for accurate repeat sUSV surveys (Figure 15). The 10-step guide is divided into three sections, Investigation of Materials (red color),

Preparation for the Survey (yellow color), and the Execution & Analysis (green color). The three sections are cohesive and flow through the entire survey process. Following each section and step properly will provide accurate bathymetric surveys using a sUSV in shallow nearshore environments. This guide will use the estuary as an example and can be implemented for other low energy wave environments.

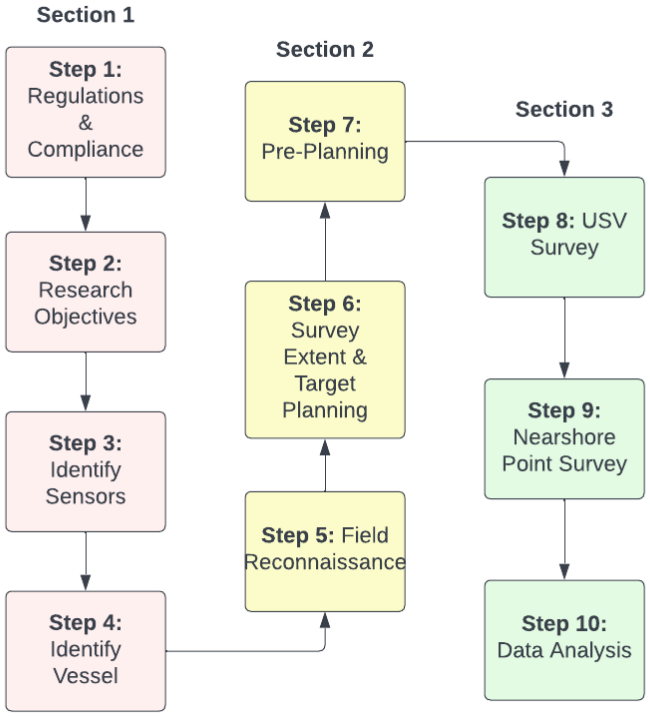

Figure 15. Step-by-step guide for sUSV surveys in low energy wave environments. Section 1: Investigation of Materials (red) covers steps 1-4. Section 2: Preparation for the Survey (yellow) covers steps 5-7. Section 3: Execution & Analysis (green) covers steps 8-10.

Section 1: *Investigation of Materials,* starts with the first step of the guide, Step 1: *Regulations & Compliance*, is to ensure the study area can accommodate the sUSV survey. This entails proper communication with the area of interest and ensuring permission from the

supervising individuals. In this study, permission from the YMCA Camp Seafarer was granted to the university for installation of wind and wave sensors as well as the sUSV surveys. Step two, Step 2: *Project Objectives*, directs the project objectives and what the outcome must be for the study. This study aimed to analyze geomorphic changes within the shallow nearshore environment with repeat sUSV surveys conducted at the same location. The next step, Step 3: *Identify Sensors*, is to analyze the equipment being used, specifically the sonar equipment. This study utilized a single beam echosounder, specifically the Seafloor Systems HydroLite-TM. The HydroLite-TM has a frequency of 200 KHz, beam width of 9 degrees, ping rate of 6 Hz, operating range of 0.3 – 75 m, and reported depth accuracy of 0.01 m (Seafloor 2020b). This was used for each survey and records one point continuously each second, where one point is collected that is one point measurement. The next step, Step 4: *Identify Vessel*, is to examine the sUSV of choice. The sUSV used for this study was the Seafloor Systems Echoboat-160 used as a remote-control vehicle. It is important to determine what type of maneuvering that will occur, whether remote or autonomous.

Once the permissions are granted, the study goal is developed, the sonar sensors are chosen, and the specific sUSV is chosen, it is time to assess the area of study for surveys. Section 2: *Preparation of the Survey*, starts with Step 5: *Field Reconnaissance*, this step requires going into the field, or examining the area of study to decide what obstacles are present. The topography and bathymetry environments must be analyzed for safe transportation of the sUSV and accompanying equipment. Examine the shoreline environment, or area of study, to find a water access entrance area for the sUSV. This could be a boat ramp, a shoreline bluff, a slow sloping grassy yard, etc. The surveyor should use caution and be prepared for any shoreline bluff conditions. It is also a good idea to use a kayak and venture out in the survey with a measuring

stick to check any unseen features below the water. This also helps with identifying whether the sUSV must be carried in the water and how far to ensure no equipment is damaged by underwater features.

Once a secure entrance to the water with the sUSV is located, it is time to see the extent of the survey area. The next step, Step 6: *Survey Extent and Target Planning*, is to designate end markers for the extent of the survey on the shoreline. This study used natural markers such as trees or shoreline features as the extent of the survey. This can be problematic when monitoring changing shorelines. It is best to implement targets that will stay secure, in the same location, for the entire study. Targets such as ground control points or rebar with a safety cap in top to remain in the same location to ensure surveys are at the same extent each time, is recommended. Now that the survey location is analyzed and the locations of ground control points are designated, it is time to ensure all pre-planning for the sUSV is complete before going back into the field for a survey. Step 7: *Pre-Planning*, includes the necessary equipment is charged, the sUSV diagnostics are completed, wind speeds, wave chop, and weather are examined, and a crew is assembled. The sUSV must be checked in the lab setting for any malfunctions that could occur and should be prioritized before a survey. Ideal boating and weather conditions must be met before a survey can be conducted. Ideal conditions include no to light wave chop, wind speeds 0-5kts, and sunny or partly cloudy skies, there must be no chance of rain or thunderstorms in the vicinity. A team of at least two people must be available for the sUSV survey. Once the ideal conditions have been met, a survey day can be planned with the crew.

The last section, Section 3: *Execution and Analysis*, starts with Step 8: *USV Survey*, the crew may begin a sUSV survey. Once the USV survey is complete, or simultaneously depending on the size of the crew, Step 9: *Nearshore Points Survey*, the accompanying nearshore reference

survey may begin. Remember to create accurate field notes to reference when processing the data. These occur strictly in the field and troubleshooting may occur due to equipment synchronization errors, but for the most part can be fixed in the field with the equipment manuals. Once the survey is complete, data processing occurs in the last step, Step 10: *Data Analysis*, this is where the field notes help if there is anything in question from the survey.

Chapter 5: Conclusion

The major objective of this study was to quantify nearshore morphological changes as depositional or erosional volume in the Neuse River Estuary using the new on-demand remote sensing device called a small Unoccupied Surface Vessel (sUSV). To achieve this objective, two Real-time Kinematic Global Navigation Satellite Systems (RTK-GNSS) and sUSV single-beam sonar surveys were carried out in February and April 2022. These datasets were used to create Bathymetric Elevation Models (BEMs) and calculate short-term volumetric changes that were matched with observed wind and wave characteristics. The February 2022 BEM was also compared with a topobathy LiDAR BEM collected in 2020 to assess any long-term changes. The results suggested that sUSVs are promising for assessing morphological changes in shallow nearshore environments where larger boating vessels are unable to reach. The following conclusions are drawn from this study:

- For each the February and April 2022 survey datasets, three BEMs were generated using Empirical Bayesian Kriging (EBK), Global Polynomial Interpolation (GPI), and Spline. EBK achieved the best result for both surveys based on conditions observed in the field as well as a Root Mean Square Error (RMSE) of 0.21 m for February and 0.16 m for April.
- The observed dominant wind speeds for February and April were on average 5-10 m/s. While both months had similar average wind speeds, their directions were different (Northeast and South directions for February and Southwest direction for April). As can be expected in a wave dominated estuary with these observed wind speeds, wave depth minimum and maximum ranges were small. The wave depth minimum and maximum 90th percentile ranged 0.05 m for February and 0.03 m for April.

- Changes in the nearshore bathymetry for the long-term (2020 to February 2022 and 2020 to April 2022) and short-term (February to April 2022) were negative resulting in erosion with no detected deposition. Bathymetry loss ranged from 0.3 to 0.69 m between February and April, and the observed wind and wave data were likely not the cause. Other factors such as currents should be investigated in the future.
- Transporting the sUSV to and from shallow nearshore estuarine environments can be challenging. The vehicle must be transported to depths at least twice the minimum value needed to detect depth soundings (e.g., minimum depth detection of 0.3 m x 2 = 0.6 m) and requires a team of two, preferably three people.
- This study provided a 10-step field workflow that integrates previous sUSV survey techniques along with experience gained in the field. Major steps included following regulations and compliance, defining the research objective(s), conducting a field reconnaissance, defining the survey extent and target planning, conducting the sUSV survey along with independent RTK-GNSS surveys, and data analysi

References

Aarts, A. A., Anderson, J. E., Anderson, C. J., Attridge, P. R., Attwood, A., Axt, J., Babel, M., Bahník, Š., Baranski, E., Barnett-Cowan, M., Bartmess, E., Beer, J., Bell, R., Bentley, H., Beyan, L., Binion, G., Borsboom, D., Bosch, A., Bosco, F. A., … Zuni, K. (2015). Estimating the reproducibility of psychological science. *Science, 349*(6251). https://doi.org/10.1126/science.aac4716

Benninger, L. K., & Wells, J. T. (1993). Sources of sediment to the Neuse River estuary, North Carolina. In *Marine Chemistry* (Vol. 43).

Clunies, G. J., Mulligan, R. P., Mallinson, D. J., & Walsh, J. P. (2017). Modeling hydrodynamics of large lagoons: Insights from the Albemarle-Pamlico Estuarine System. *Estuarine, Coastal and Shelf Science, 189*, 90–103. https://doi.org/10.1016/j.ecss.2017.03.012

Corbett, D. R. (2010). Resuspension and estuarine nutrient cycling: Insights from the Neuse River Estuary. *Biogeosciences*, *7*(10), 3289–3300. https://doi.org/10.5194/bg-7-3289-2010

Dalrymple, R. W., Zaitlin, B. A., & Boyd, R. (1992). *PERSPECTIVE ESTUARINE FACIES MODELS: CONCEPTUAL BASIS AND STRATIGRAPHIC IMPLICATIONS l*. http://pubs.geoscienceworld.org/sepm/jsedres/article-pdf/62/6/1130/2811129/1130.pdf

Doneus, M., Miholjek, I., Mandlburger, G., Doneus, N., Verhoeven, G., Briese, C., & Pregesbauer, M. (2015). Airborne laser bathymetry for documentation of submerged archaeological sites in shallow water. *International Archives of the Photogrammetry, Remote Sensing and Spatial Information Sciences - ISPRS Archives*, *40*(5W5), 99–107. https://doi.org/10.5194/isprsarchives-XL-5-W5-99-2015

El-Hattab, A. I. (2014). Single beam bathymetric data modelling techniques for accurate maintenance dredging. *Egyptian Journal of Remote Sensing and Space Science*, *17*(2), 189–195. https://doi.org/10.1016/j.ejrs.2014.05.003

Elder, W. P. (2013). Bedrock geology of the San Francisco Bay Area: A local sediment source for bay and coastal systems. *Marine Geology, 345*, 18–30. https://doi.org/10.1016/j.margeo.2013.02.006

esri. (n.d.). *How Global Polynomial Interpolation Works*. https://pro.arcgis.com/en/pro-app/2.7/help/analysis/geostatistical-analyst/how-global-polynomial-interpolation-works.htm#:~:text=Global polynomial interpolation fits a,scale pattern in the data

Felix Rohrbach. (2015, October 14). *Point Density and Point Spacing* . https://felix.rohrba.ch/en/2015/point-density-and-point-spacing/

Harris, P. T. (2012). Seafloor Geomorphology-Coast, Shelf, and Abyss. In *Seafloor Geomorphology as Benthic Habitat* (pp. 109–155). Elsevier Inc. https://doi.org/10.1016/B978-0-12-385140-6.00006-2

Horta, J., Pacheco, A., Moura, D., & Ferreira. (2014). Can recreational echosounder-chartplotter systems be used to perform accurate nearshore bathymetric surveys? *Ocean Dynamics*, *64*(11), 1555–1567. https://doi.org/10.1007/s10236-014-0773-y

Laird, M. P., Theberge, B. L., & Jones, N. B. (1975). *An Assessment of Estuarine and Nearshore Marine Environments*. https://doi.org/10.21220/V5F161

Matsuba, Y., & Sato, S. (2018). Nearshore bathymetry estimation using UAV. *Coastal Engineering Journal*, *60*(1), 51–59. https://doi.org/10.1080/21664250.2018.1436239

Met One Instruments, I. (2001). *Met One Instruments, Inc 034B WIND SENSOR OPERATION MANUAL*. www.metone.com

Mulligan, R. P., Mallinson, D. J., Clunies, G. J., Rey, A., Culver, S. J., Zaremba, N., Leorri, E., & Mitra, S. (2019). Estuarine Responses to Long-Term Changes in Inlets, Morphology, and Sea Level Rise. *Journal of Geophysical Research: Oceans*, *124*(12), 9235–9257. https://doi.org/10.1029/2018JC014732

Muzirafuti, A., Barreca, G., Crupi, A., Faina, G., Paltrinieri, D., Lanza, S., & Randazzo, G. (2020). The contribution of multispectral satellite image to shallowwater bathymetry mapping on the Coast of Misano Adriatico, Italy. *Journal of Marine Science and Engineering*, *8*(2). https://doi.org/10.3390/jmse8020126

NOAA. (2016). *Hydrographic Survey Data*. National Ocean Service. https://nauticalcharts.noaa.gov/data/hydrographic-survey-data.html

NOAA. (2021, February 26). *Classifying Estuaries: By Geology*. National Ocean Service Website. https://oceanservice.noaa.gov/education/tutorial_estuaries/est04_geology.html

Orescanin, M. M., Coughlin, J., & Young, W. R. (2021). Morphological response of variable river discharge and wave forcing at a bar-built estuary. *Estuarine, Coastal and Shelf Science*, *258*. https://doi.org/10.1016/j.ecss.2021.107438

Phillips, J. D. (2022). Geomorphology of the fluvial–estuarine transition zone, lower Neuse River, North Carolina. *Earth Surface Processes and Landforms*. https://doi.org/10.1002/esp.5362

R. Davidson-Arnott. (2011). 3.04 Wave-Dominated Coasts. *Trestise on Estuarine and Coastal Science* , *Volume 3*, 73–116. https://doi.org/10.1016/B978-0-12-374711-2.00305-3

Reide Corbett, D., Walsh, J. P., Cowart, L., Riggs, S. R., Ames, D. V, & Culver, S. J. (2008). *Shoreline change within the albemarle-Pamlico eStuarine SyStem, north carolina Department of geological Sciences thomas harriot college of arts and Sciences and institute for coastal Science and Policy east carolina university*.

Seafloor Systems Incorporated. (2022). *HydroLite-TM Data Sheet*. https://www.seafloorsystems.com/singlebeam

Smith, P. A. (1935). *OCEANOGRAPHIC ACTIVITIES OF THE UNITED STATES COAST AND GEODETIC SURVEY*. https://doi.org/10.1029/TR016i001p00216

Specht, M., Specht, C., Szafran, M., Makar, A., Dabrowski, P., Lasota, H., & Cywiński, P. (2020). The use of USV to develop navigational and bathymetric charts of yacht ports on the example of National Sailing Centre in Gdańsk. *Remote Sensing*, *12*(16). https://doi.org/10.3390/RS12162585

The Submarine Signal Fathometer for Visual Echo Soundings. (1930).

Vallé, B. L., & Pasternack, G. B. (2006). Field mapping and digital elevation modelling of submerged and unsubmerged hydraulic jump regions in a bedrock step-pool channel. *Earth Surface Processes and Landforms*, *31*(6), 646–664. https://doi.org/10.1002/esp.1293

APPENDIX A: sUSV Setup

Appendix A is divided into three parts for the sUSV setup. The first part is the preparation, before entering the field, the second is the in-field procedures, and the third is the post-field procedures to maintain equipment.

Part 1: Preparation-Before Entering the Field Setting

Ensure all materials are charged (if required), tested (if required), and ready to go (Figure 12) before a planned survey date.

1. (4) 14.8v batteries
2. (2) Data collectors
3. Echosounder
4. Spectra Precision batteries
5. Remote control batteries
6. Field laptop (if checking measurements in the field is needed)
7. Base station tripod
8. Rover poles
9. Echosounder pole
10. Spectra Precision Base
11. (2) Spectra Precision Rover
12. Transducer
13. Kayak (only needed if survey location must utilize a kayak for sUSV transportation on the water)

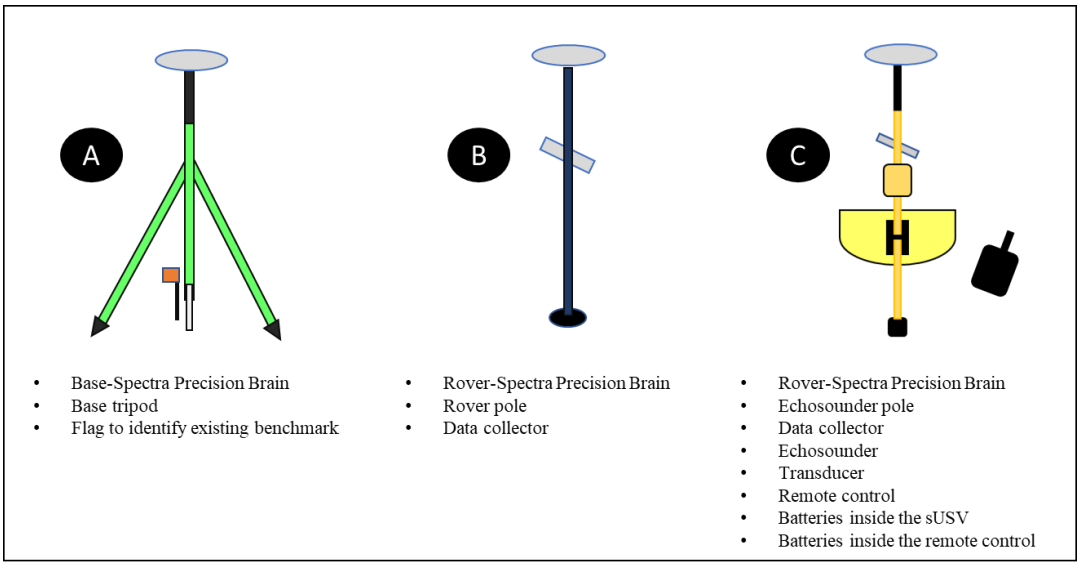

Figure A1. Diagrams of the equipment for the field setting with needed materials listed underneath. A: represents the base station set-up, B: represents the rover unit used for nearshore survey points for accuracy testing, and C: represents the sUSV set-up.

A thruster test must occur before entering the field for a survey. Be sure to indicate any complications before going to a survey location.

Conduct a Thruster Test:

- Plug in the four 14.8v batteries in the designated slots in the sUSV
- Turn on the remote control
- Once the Seafloor screen goes away hold the left joystick down for a few seconds and release
- Turn on the sUSV by the port and starboard switches on the stern (back of the boat)
- Once the sUSV is running, wait 10 seconds and move the joysticks to see if the thrusters move, going in the forward and backward directions with the controller
- If the thrusters work, great, turn off the sUSV and then the controller
- If the thrusters do not work follow these instructions or use the calibration card and program with the numbers on the last page of the ESC Calibration PDF that came with the sUSV
- If the above does not work, contact Seafloor Systems and describe what is going on.

Once the sUSV is working properly and all materials are charged and loaded into a transportation vehicle, a survey may be completed.

Part 2: Field Setting Procedure

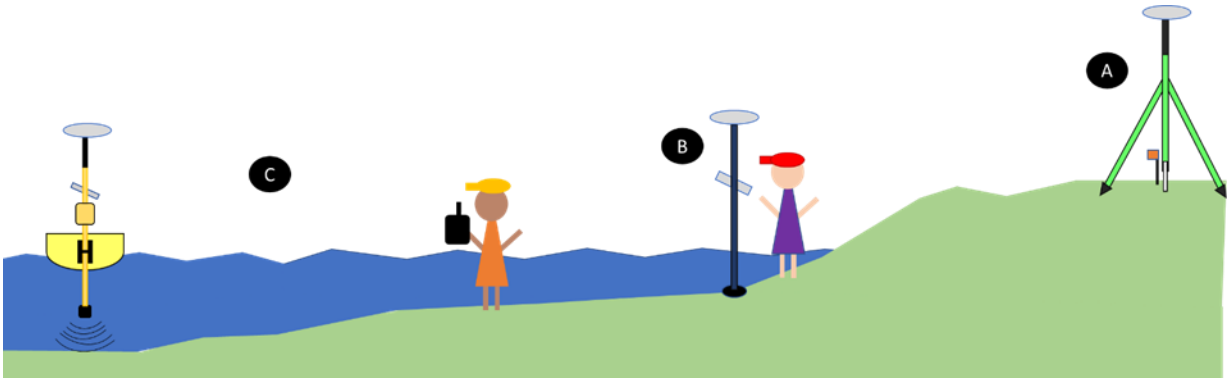

Figure A2. This is what field surveys should look like. A: The base station, B: The nearshore survey points being measured, and C: Someone controlling the sUSV. The green mass is land and the blue mass is the water.

1. Ensure the field setting (Figure 13) is similar for each survey
2. Unload the truck
3. Carry the RTK-GNSS base station materials to the established benchmark or create a benchmark
    3.1. Set up the base station materials and begin recording
    3.2. Measure the height of the base station (this will be needed for a future step)
    3.3. Make someone in charge of the base station batteries (needs to be checked every 2 hours)
4. Carry the sUSV materials to the launching location
5. Carry the RTK-GNSS materials needed for the elevation/comparison measurements
    5.1. Assemble the rover
        5.1.1. Make sure to grab the flat end to attach to the rover pole
        5.1.2. Set up the rover balance poles
        5.1.3. Attach the Trimble brain to the top of the rover pole
        5.1.4. Attach the Carlson data collector
    5.2. Begin surveying points
        5.2.1. Survey points in the nearshore where the sUSV cannot survey
        5.2.2. Survey points where the sUSV starts surveying and the person carrying the pole can still touch without getting the materials in the water (20)
6. Complete the "Thruster Test" , again, before securing the hull lid
7. Assemble the SBES materials (Figure 13)
    7.1. Attach 2 poles to the stern
        7.1.1. The pole with two pieces of tape (used for the same measurement markings for each survey) goes through the stern piece. Make sure the part of the pole that is facing the ground is the end that the transducer can screw into.
        7.1.2. The other pole then screws on top of the other, going to the sky.
        7.1.3. Attach both poles by securing the stern piece with the screws and the hex key wrench
    7.2. Screw on the transducer (this is easier to attach to the pole with two pieces of tape on it before securing the poles to the stern
    7.3. Velcro the SBES above the stern near the black metal piece attached to the top of the sUSV
    7.4. Attach the Carlson data collector above the SBES

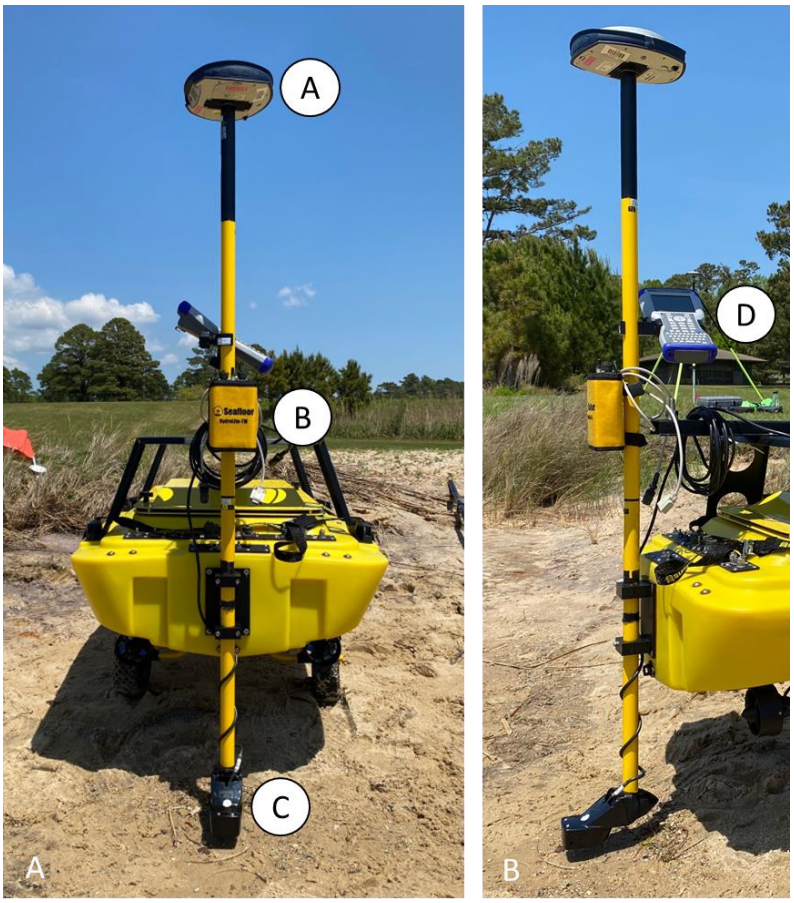

Figure A3. Image on the left, A: Rover brain. B: Echosounder, and C: Transducer. Image on the right, D: Data colletor. All materials are attached to the yellow echosounder pole.

8. Attach the Trimble brain to the top of the secured stern pole
9. Turn on the Trimble brain and the data collector, begin the wireless connection to the base station from the data collector, and once the base is connected, begin the connection to the rover from the data collector.
10. Carry the sUSV to the blue kayak in the water (used to transport the sUSV to an area it will not be damaged when surveying)
11. Once at the desired location for surveying
    - 11.1. Take the sUSV off the kayak (if the kayak is needed for transportation)
    - 11.2. Assemble data collector items
    - 11.3. Make sure the transducer cord is plugged into the power port on the SBES before the data collector cord is plugged into the other port
    - 11.4. Begin surveying
12. There should be a person in control of the sUSV in the water moving while creating transects perpendicular to the shore (do this until the end of the survey area)

13. When going back to the launch location, the person in control of the sUSV will signal for battery change for the sUSV
14. Someone needs to bring the batteries form the shore and help change batteries in the water
15. When new batteries are in, begin the transects parallel to shore and have someone in a kayak (if needed, as far out as the sUSV can go to keep the person in control in line until they can reach the area where they can touch) (see images below).

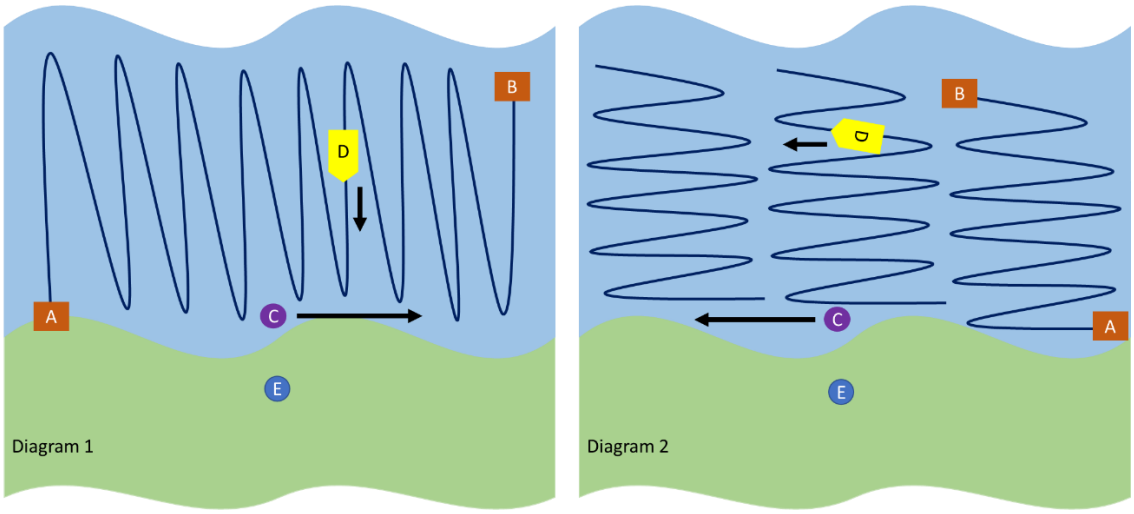

Figure A4. The cross-hatch method used when conducting bathymetric survey S, where A = starting point, B = ending point, C = person in control of the sUSV, D = the sUSV, E = base station location, and the arrows indicate the direction in which C or D are moving within the survey. The green mass is land and the blue mass is the nearshore waters. Diagram 1 (left) shows the sUSV being maneuvered perpendicular to shore from point A to point B and the person in control is moving to the right while controlling the sUSV. Diagram 2 (right) shows the sUSV being maneuvered parallel to shore from point A to point B (repeating) until the survey is complete and the person in control is moving to the left as the survey continues

16. Conduct transects until the launch point is reached
17. Once the survey is complete
    17.1. Turn off the EchoBoat, then the remote control
    17.2. Close the data collector screen and save
    17.3. Turn off the Trimble brain
    17.4. Take the SBES pole off
    17.5. Push the EchoBoat back to shore and place on the kayak holder
18. Take apart equipment
19. Place materials in the designated boxes or containers for traveling
20. Pack up truck

Part 3: Storage of Materials

1. Place the batteries of the sUSV in storage mode
2. Rinse the sUSV of the saltwater (around the thrusters and where salt residue is showing)
3. Rinse the transducer and poles that were in the saltwater

4. Set the transducer and poles out to dry properly
5. The next day make sure everything is dry and in the correct storage settings and pack everything up for the next survey to keep the lab space clean and organized.